AD-A061 520 PERKIN-ELMER CORP NORWALK CONN ELECTRO-OPTICAL DIV F/G 20/5
INSTRUMENTATION FOR A FIELDABLE REMOTE-SENSING CO2 LASER SYSTEM--ETC(U)
AUG 76 R B MCINTOSH DAAA15-75-C-0139
UNCLASSIFIED PE-13007 ED-CR-76089 NL

END
DATE FILMED
1-79
DDC

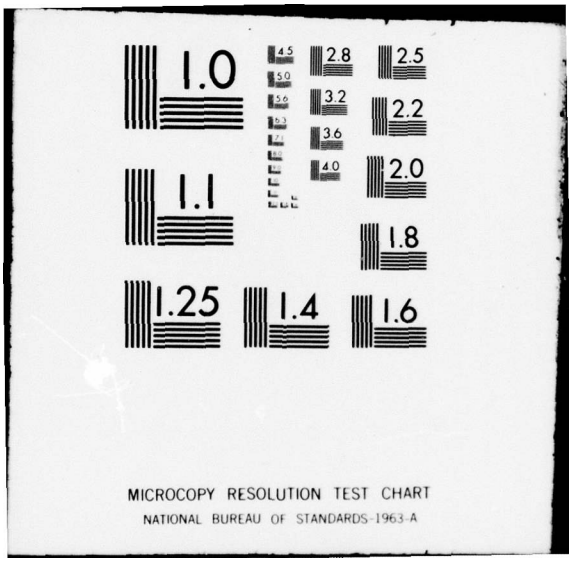
1.0
1.1
1.25
1.4
1.6
1.8
2.0
2.2
2.5
2.8
3.2
3.6
4.0
4.5
5.0
5.6
MICROCOPY RESOLUTION TEST CHART
NATIONAL BUREAU OF STANDARDS-1963-A

UNCLASSIFIED

SECURITY CLASSIFICATION OF THIS PAGE *(When Data Entered)*

REPORT DOCUMENTATION PAGE

READ INSTRUCTIONS BEFORE COMPLETING FORM

1. REPORT NUMBER: ECOM-76089	2. GOVT ACCESSION NO.
3. RECIPIENT'S CATALOG NUMBER	
4. TITLE (and Subtitle): INSTRUMENTATION FOR A FIELDABLE REMOTE-SENSING CO_2 LASER SYSTEM.	5. TYPE OF REPORT & PERIOD COVERED: Final Report. May 1975 - May 1976.
6. PERFORMING ORG. REPORT NUMBER: PE-13007	
7. AUTHOR(s): Robert B. McIntosh, Jr.	8. CONTRACT OR GRANT NUMBER(s): DAAA15-75-C-0139
9. PERFORMING ORGANIZATION NAME AND ADDRESS: The Perkin-Elmer Corporation, Electro-Optical Division, Norwalk, Connecticut 06856	10. PROGRAM ELEMENT, PROJECT, TASK AREA & WORK UNIT NUMBERS
11. CONTROLLING OFFICE NAME AND ADDRESS: Commander, Edgewood Arsenal, Attn: SAREA-TS-R, Aberdeen Proving Ground, Maryland 21010	12. REPORT DATE: August 1976 13. NUMBER OF PAGES: 69
14. MONITORING AGENCY NAME & ADDRESS *(if different from Controlling Office)*: Commander, Edgewood Arsenal, Attn: SAREA-DE-DDR, Aberdeen Proving Ground, Maryland 21010 (CPO V. J. Cannaliato 671-3884)	15. SECURITY CLASS. *(of this report)*: UNCLASSIFIED 15a. DECLASSIFICATION/DOWNGRADING SCHEDULE: NA

16. DISTRIBUTION STATEMENT *(of this Report)*

Approved for public release; distribution unlimited.

12 69p.

17. DISTRIBUTION STATEMENT *(of the abstract entered in Block 20, if different from Report)*

DDC RECEIVED NOV 27 1978

18. SUPPLEMENTARY NOTES

19. KEY WORDS *(Continue on reverse side if necessary and identify by block number)*

CO_2 laser	Pulse width	Power requirements
Laser transmitter	Integrated system	Operation instructions
Laser receiver	Range safety	Maintenance instructions
Signal processing	Voltage safety	Grating alignment
Power measurements	Eye safety	

20. ABSTRACT *(Continue on reverse side if necessary and identify by block number)*

A spectrally tunable IR laser transmitter and a 30-cm f/4.0 laser receiver using a (PbSn)Te cooled detector were developed and tested. A design for signal-processing electronics and a system control console were submitted, ~~to Edgewood Arsenal~~. The Q-switched laser sequentially emits at eight selected wavelengths in a pulse train repeating 100 times per sec. Laser scattered or reflected energy from distant natural targets is collected by the receiver. Absorption characteristics of the return beam are compared with those from potential chemical —

279 560

DD FORM 1 JAN 73 1473 EDITION OF 1 NOV 65 IS OBSOLETE

78 11 15 135

UNCLASSIFIED

SECURITY CLASSIFICATION OF THIS PAGE *(When Data Entered)*

20. ABSTRACT

agents. Signal-processing electronics and a PDP/11 computer identify and measure the concentration of an agent using its unique absorption spectrum.

PREFACE

This final report is a comprehensive summary of all work accomplished under U.S. Army, Edgewood Arsenal Contract No. DAAA15-75-C-0139 from its initiation on 19 May 1975 through 30 April 1976.

The use of trade names in this report does not constitute an official indorsement or approval of the use of such commercial hardware or software. This report may not be cited for purposes of advertisement.

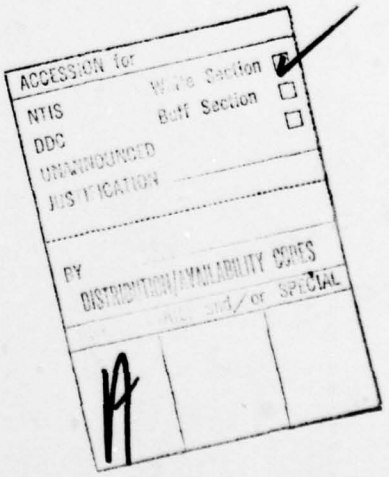

FOREWORD

For a number of years, Edgewood Arsenal has been evaluating long-path infrared detection techniques for sensing chemical agent gas clouds. Experience gained from the operation of a breadboard CO_2 laser system and the results of studying the spectral absorption of chemical agents along with potential interferences has demonstrated the feasibility of an active laser system concept. The purpose of this contract was to design, fabricate, and test a fieldable CO_2 laser sensor system to be used by Edgewood Arsenal personnel. If field test data confirms this technical approach, it may be used to support continued sensor development leading toward battiefield deployable instrumentation.

TABLE OF CONTENTS

LIST OF ILLUSTRATIONS

INSTRUMENTATION FOR A FIELDABLE REMOTE-SENSING CO^2 LASER SYSTEM

1. INTRODUCTION

The objective of this program was to design, build and demonstrate a fieldable, remote-sensing, CO_2 laser system for the U.S. Army, Edgewood Arsenal. The system designed and tested under this contract consisted of a spectrally tunable infrared laser transmitter and a 30-cm diameter, f/4.0 laser receiver utilizing a (PbSn)Te cooled detector. In addition, a detailed design for signal-processing electronics and a system control console were submitted to Edgewood Arsenal for concurrent fabrication and assembly.

The Q-switched laser sequentially emits energy at eight selected wavelengths in a pulse train that repeats 100 times per second. Laser energy reflected or scattered from distant natural-terrain objects is collected by the receiver. The return beam is monitored for changes in absorption along a 1-kilometer path between laser lines tuned on and off absorption frequencies of potential chemical agents. The signal-processing electronics measures the concentration path length product of an agent using its unique absorption spectrum.

During the initial phase of the contract, a review was made of past CO_2 laser work sponsored by Edgewood Arsenal, as well as appropriate work reported in open literature. This information served as a basis for further study and for the selection of an optimum system approach. Tradeoff analysis of applicable performance parameters were then undertaken. The Appendix to this report summarizes the results of alternate laser, receiver, and detector performance evaluations. Approval to fabricate and assemble the recommended system using a grating-tuned CO_2 laser and direct detection receiver was given at the critical design review meeting held at Perkin-Elmer on 5 September 1975.

During March 1976, subsystem tests were performed on the laser transmitter and receiver prior to final integrated-system testing conducted with Edgewood Arsenal personnel in April. Laser tuning was demonstrated with both $^{12}C^{16}O_2$ and $^{13}C^{16}O_2$ gas mixtures. A field test with the laser filled with the common CO_2 isotope mixture indicated that the system met or exceeded all contract sensitivity objectives. Stable laser operation was demonstrated on 54 or 52 lines of $^{12}C^{16}O_2$ between 9.26 and 10.81 microns. Laser operation was also demonstrated on 17 rotational levels of the R-branch of the 00°1 - 10°0 vibrational band of $^{13}CO_2{}^{16}$. Attempts at lasing on the $^{13}CO_2{}^{16}$ 00°1 - 02°0 vibration band were unsuccessful. This result may possibly be attributed to the fact that the laser gain at ambient temperature is less than that of water-cooled units.

Table 1 is a summary of the major system performance parameters for the equipment.

TABLE 1. SYSTEM PERFORMANCE SUMMARY

Peak laser power:	500 to 2,000 watts
Average laser power/line:	30 milliwatts
Laser pulse width:	<250 nanoseconds
Tunable spectral range:	9.26 to 10.81 microns
Number of independently selectable lines:	8
Laser beam divergence:	<2.5 milliradians
Receiver optics:	30-cm dia., f/4.0
Receiver field-of-view (FOV):	2.5 milliradians
Receiver noise equivalent power (NEP):	1.5×10^{-11} watts
System signal-to-noise ratio: (1 kilometer range, 0.01% reflector, 10% absorption)	8:1
Laser transmitter:	
-Weight	54 kg
-Size	190-cm x 39.5-cm dia. (max. envelope)
Laser receiver:	
-Weight	39 kg
-Size	155-cm x 40-cm dia.

2. LOPAIR SYSTEM DESCRIPTION

2.1 FUNCTIONAL DESCRIPTION

The CO_2 laser transmitter shown in Figure 1 is excited by maintaining an electrical discharge between two electrodes mounted at either end of a sealed ceramic plasma tube. A rotating scan mirror is used to sequentially Q-switch and grating-tune the laser. Eight short-duration pulses are emitted during each revolution of the scan mirror as sequential alignment is achieved between the output coupling mirror and eight diffraction gratings. The frequency of the eight output pulses is independently adjustable by setting the Littrow angle of each grating to a wavelength corresponding to one of the CO_2 vibration-rotation lines.

A pyroelectric reference detector samples transmitted laser power by monitoring the reflection off one of the two Brewster windows. Laser radiation is collimated by a 2.5X ZnSe beam expander and transmitted to a distant terrain feature. A 16X telescope and HeNe laser mounted on the side of the laser assist in laser alignment and pointing. Scan mirror position and speed data is obtained from a rotary encoder coupled to the scan mirror drive motor.

Reflected or scattered laser radiation is collected by the 30-cm diameter Newtonian telescope shown in Figure 2. The telescope infrared focus is relayed to a liquid-nitrogen-cooled (PbSn)Te detector with a cooled filter and fieldstop inside a stainless-steel dewar. A dichroic beamsplitter, crosshair reticle, and eyepiece provide a visual image for boresighting the telescope.

The system control/display console houses the signal processing and laser control electronics in separate drawers. A dual-beam oscilloscope and the Hipotronics high-voltage power supply, required to excite the laser, are also mounted in the console unit. Power supplies used to operate the signal and reference detectors are mounted in the processing electronics drawer, and a variable dc supply required to drive the scan motor is associated with the laser control circuitry.

2.2 CO_2 LASER LOPAIR SENSOR CONCEPT

The CO_2 laser is a discretely tunable laser whose output is alternately tuned to lie on and off an absorption frequency of a particular molecular absorbing gas. Assuming that the respective wavelengths, λ_{on} and λ_{off}, are reasonably close ($\lambda_{on}-\lambda_{off} << \lambda_{on}$), one can conclude that the atmospheric attenuation due to scattering (Rayleigh and Mie) is the same for both wavelengths. The total attenuation suffered by the laser's radiation as it passes through the atmosphere can be expressed as $\alpha(\lambda)$, where:

$$\alpha(\lambda) = a(\lambda) + s(\lambda) \qquad (1)$$

The term $a(\lambda)$ corresponds to the attenuation coefficient due to absorption, while the term $s(\lambda)$ represents the attenuation due to scattering. Since $s(\lambda)$

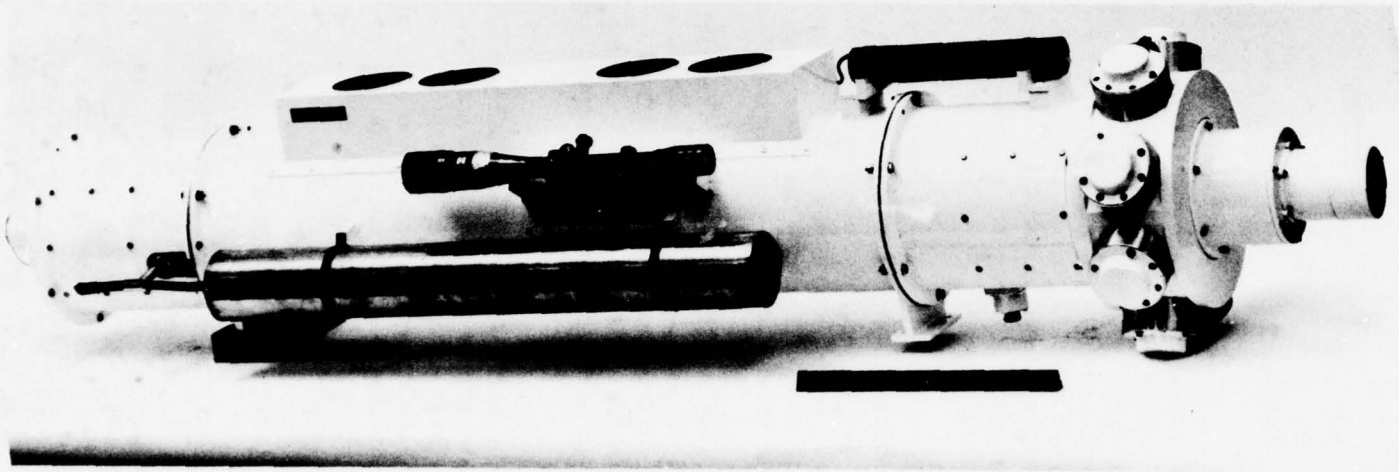

Figure 1. CO_2 Laser Transmitter

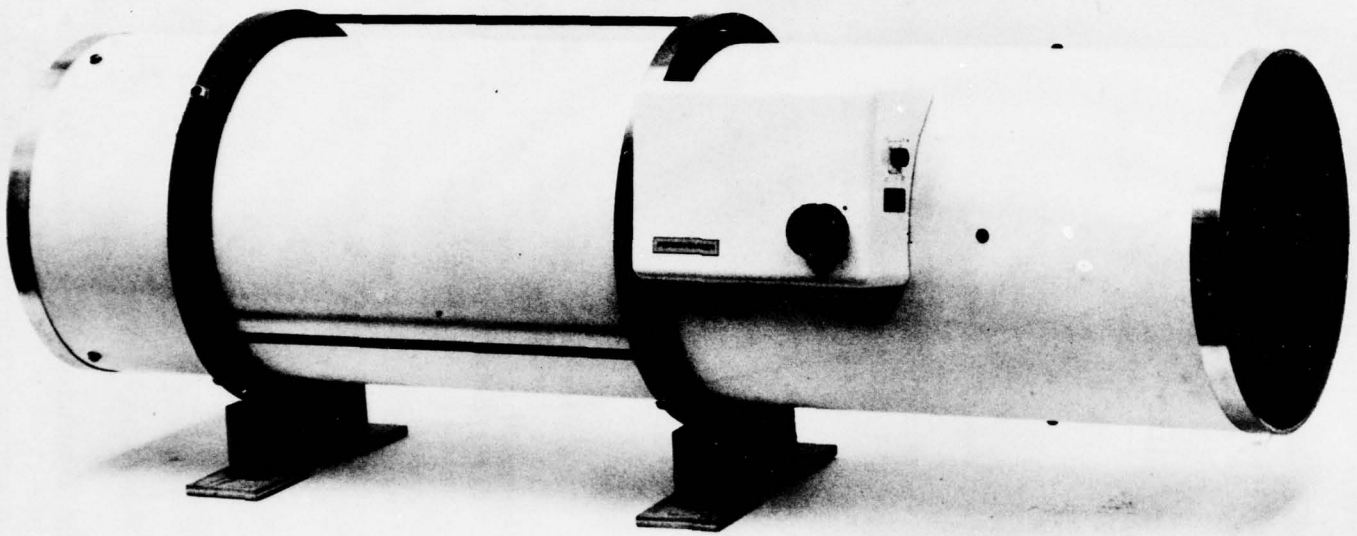

Figure 2. Laser Receiver

is a weak function of wavelength, the assumption that $s(\lambda_{on}) \cong s(\lambda_{off})$ is reasonable. However, the absorption coefficient varies greatly with wavelength. Judicious choice of laser output wavelengths will allow measurement of the concentration of the absorbing gas.

In the laser detection technique, the laser transmits energy into the atmosphere; and backscattered (reflected) signal from a Lambertian reflector of reflectivity ρ is shown to be

$$P_s(R) = \frac{\xi \rho A P_\ell}{\pi R^2} \exp\left[-2 \int_o^R \alpha(r)dr\right] \tag{2}$$

where:

P_ℓ = the transmitted laser power (W)

A = telescope effective aperture area (m^2)

R = range to the reflector (m)

ξ = optical efficiency of the receiver

$\alpha(r)$ = the total attenuation coefficient of the atmosphere at range r

The factor 2 in the exponent accounts for the fact that the laser radiation makes one round-trip between the transmitter and receiver. This active laser detection technique can be extended to the detection of several different and spectrally interfering gases with the aid of additional laser frequencies and appropriate multispectral data analysis.

Consider first the power received when the laser is tuned off resonance at a wavelength of no absorption by the gas to be detected. The signal power is:

$$P_s^{off} = (\xi \rho A/\pi R^2) P_\ell \exp\left[-2 \int_o^R s(r)dr\right] \tag{3}$$

where s(r) is the attenuation coefficient (m^{-1}) due to scattering over the small range increment dr about range r. Assuming that s(r) is constant over the entire sample region, this exponential term can be replaced by a simple constant (T_s) where

$$T_s = \exp[-sR], \tag{4}$$

the one way transmittance of the atmosphere.

An empirical relation for the Mie scattering coefficient (Rayleigh scattering is negligible at 10μm) is given by[1]

$$s(\lambda) = (3.91/V)(0.55/\lambda)^{0.585V^{1/3}} \quad (km^{-1}) \tag{5}$$

where V is the visibility (km) and λ is the wavelength in microns. At 10 μm, the value of $s(\lambda)$ is 0.043 km^{-1} for a visibility of 5 km. The one-way transmittance $T_s = 0.958$; the two-way transmittance to be used in Eq. (3) is therefore $0.918 \approx 0.92$.

The power received when the laser is tuned on resonance assuming $P_\ell(\lambda_{on}) = P_\ell(\lambda_{off})$] is given by

$$P_s^{on} = (\xi\rho A/\pi R^2) P_\ell T_s^2 \exp\left[-2\int_o^R a(r)dr\right] \tag{6}$$

where a(r) is the attenuation due to absorption by the chemical agent over the small range increment dr about range r. Again let us simplify the expression for absorption for computational purposes and let

$$T_a = \exp[-aR] \tag{7}$$

where a is assumed to be uniform over R. The difference in power received on and off resonance is now a measure of the gas concentration since

$$P_s^{off} - P_s^{on} = P_s^{off}\left\{1-T_a^2\right\}. \tag{8}$$

We have implicitly assumed here that the gas to be detected is not normally present in the atmosphere and has no similarity at the sampled wavelengths to possible interferants. Such cases can be handled[1] but are not discussed here.

A differential absorption of 10 percent implies that

$$(P_s^{off} - P_s^{on})/P_s^{off} = 0.1$$

$$\text{or } T_a^2 = 0.9$$

In order to detect the change in received power due to differential absorption with a given S/N we require

1. R.L. Byer and M. Garbuny, "Pollutant Detection by Absorption Using Mie Scattering and Topographic Targets as Retroreflectors," Appl. Optics, 12, pp. 1496-1505 (1973).

$$P_s^{off}\left\{1-T_a^{\,2}\right\} = \left(\frac{S}{N}\right) P_N \qquad (9)$$

where P_N is the noise power associated with the detection method utilized. The laser power needed to achieve a particular S/N is found by substituting Eq. (3) in Eq. (9), giving

$$P_\ell = \left(\frac{S}{N}\right) P_N \, \pi R^2 / \left\{\xi \rho A T_s^{\,2}(1-T_a^{\,2})\right\} \qquad (10)$$

The differential signal change on and off resonance (ΔT) is represented by the term in brackets; that is

$$\Delta T = (1-T_a^{\,2})$$

The laser power is clearly a strong function of the required measurement accuracy for a given signal change. Typically, for a laser operating in pulse mode, a peak power of 500 watts is sufficient for anticipated measurements.

2.3 LASER TRANSMITTER

The laser transmitter consists of six subassemblies: laser tube assembly (674-0079), central housing (674-1199), two end housings (674-1177 and 674-1166), grating tuner assembly (674-0076), and collimator assembly (674-0081), which houses the beam-expansion optics.

The laser tube assembly comprises a ceramic plasma tube and the two attached electrode housings, heat dissipator assemblies, and Brewster angle windows bonded to pyrex-to-kovar seals. A center support and two flexure mounts support this tube assembly inside the central housing.

Four Rotron fans are mounted in a fan manifold located on top of the central housing. Air is drawn through screened ports at the bottom of the central housing, across the laser tube, and to the finned heat-exchangers, exhausting it out the top of the fan manifold. The two end housings are flange-bolted and pinned to the central housing.

The end housings protect and provide access to the laser electrode housings and Brewster windows. Large covered ports are located in the side of each end housing to permit cleaning of the Brewster windows and to allow high-voltage lead connection. Smaller gasketed ports serve as feedthroughs for the high-voltage lead and its return. The partially transparent laser output coupling mirror, in its adjustable mount, and the collimator assembly are bolted to the second end housing. The other end housing provides a mount for the pyroelectric reference detector.

Eight grating modules are equally spaced around the outside surface of the grating tuner assembly. The assembly also houses and provides mounting for the scan mirror, its drive motor, and the rotary encoder. The HeNe alignment laser and alignment telescope are mounted in "V" blocks welded to the central tube and high-voltage end housing.

2.3.1 Laser Tube Assembly

The laser tube assembly shown in Figure 3 was designed for a sealed lifetime of 2,000 hours. The assembly features a beryllium oxide plasma tube, platinum-plated nickel electrodes, and ZnSe Brewster windows. The plasma tube (674-0134) was fabricated from two lengths of beryllium oxide tubing having a 1-cm diameter bore. The lengths of the two segments are 38 and 48 cm, respectively, which places their welded coupling sufficiently off-center to allow attachment of the center support assembly (674-0029) at the midpoint of the tube. Figure 4 shows the details of the welded coupling, center support assembly, and heat dissipating radiators (674-0082).

The two electrodes were fabricated by forming 0.58 cm, 99.98% pure nickel into 7.6-cm long x 7.6-cm diameter cylinders. The electrodes were then plated with platinum to a thickness of 0.006 cm. The electrodes are welded to the high voltage feedthrough terminals that are mounted in the end-plate of the cylindrical stainless-steel electrode housing as shown in Figure 5. Also shown is the pyrex-to-kovar seal to which the ZnSe Brewster window is cemented.

The laser tube assembly is supported in a 20-cm diameter aluminum central housing (674-1199) by means of two flexure assemblies (674-0214) and the center support. The flexure assembly consists of a large diameter, stainless steel, spoked disk and the attached G-10 fiberglass ring shown in Figure 5. To provide additional insulation, a strip of 0.02-cm mylar was placed between the flexure assembly and the electrode housing. Initially, it was planned to use identical flexure assemblies at both the high and low voltage ends of the laser tube. However, due to voltage breakdown across the fiberglass insulating ring, the flexure at the high-voltage end was later entirely fabricated from fiberglass.

Two small-bore glass return tubes are used to equalize any pressure differential that may develop along the plasma tube during laser operation. The tubes shown in Figure 3 are connected to the electrode housing via small pyrex-to-kovar seals. An insulated termination is welded to the side of the low-voltage electrode to provide a connection to the reservoir assembly via a tee-joint and flexible stainless-steel tubing.

The reservoir assembly (674-0081) was fabricated from a 76-cm x 8.9-cm diameter stainless-steel tube and end plates. All machining was done with sulfur-free oil, and attachments and seams were TIG welded. One end of the reservoir is connected to the laser tube assembly by flexible stainless-steel tubing. A DV16 thermocouple pressure gauge is mounted internally and supported to the end plate at the other end of the reservoir. Prior to attachment to the laser tube assembly, the reservoir was leak-checked and vacuum-baked.

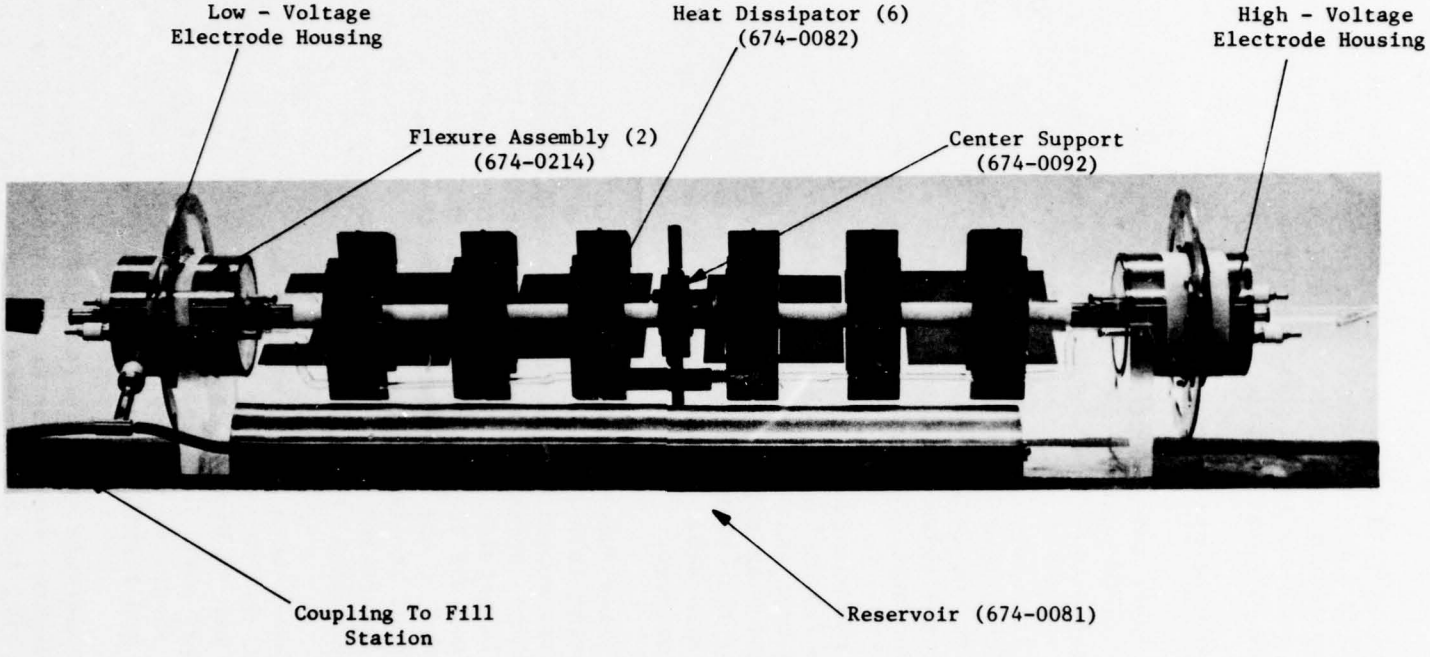

Figure 3. Laser Tube Assembly

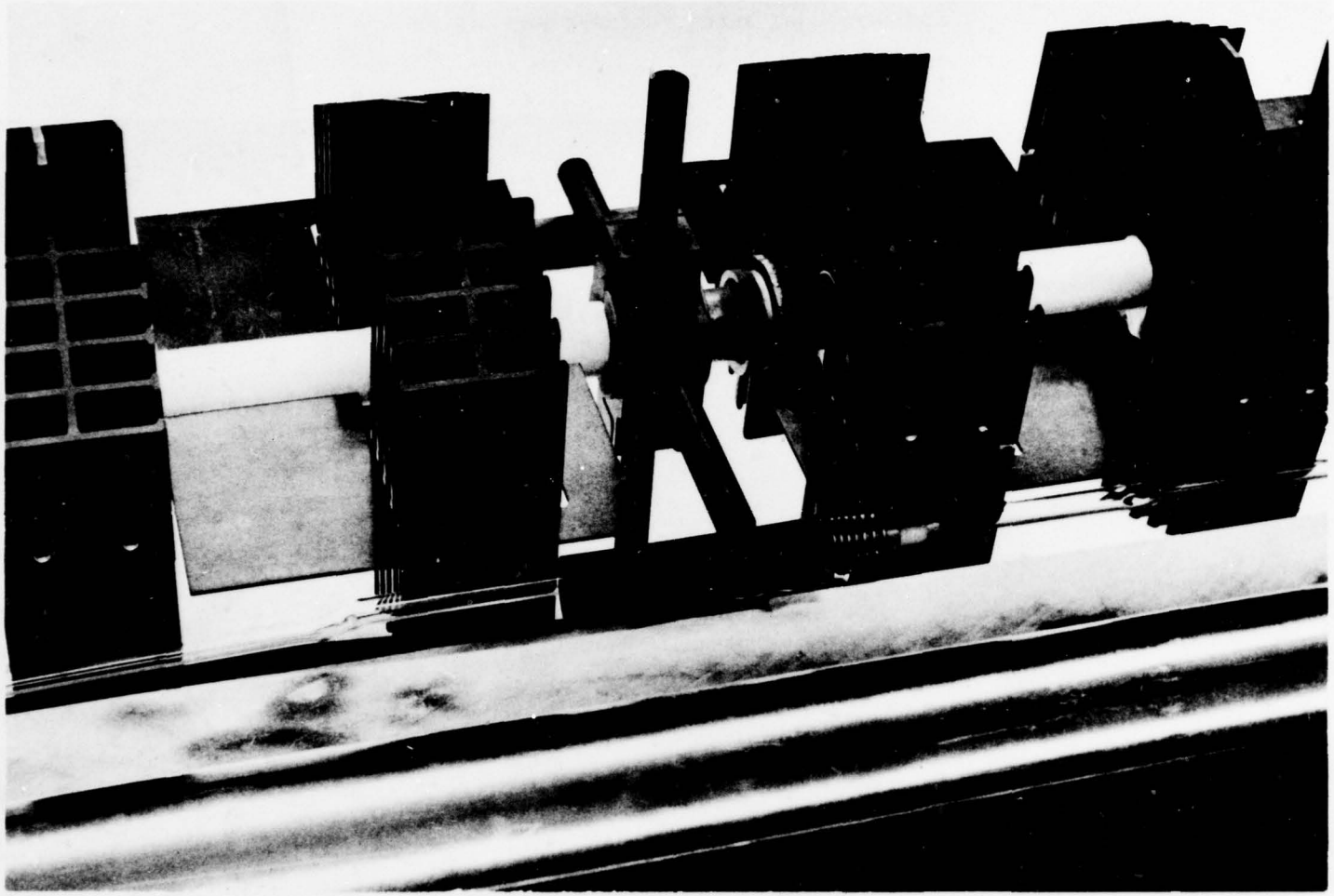

Figure 4. Midsection, Laser Tube Assembly

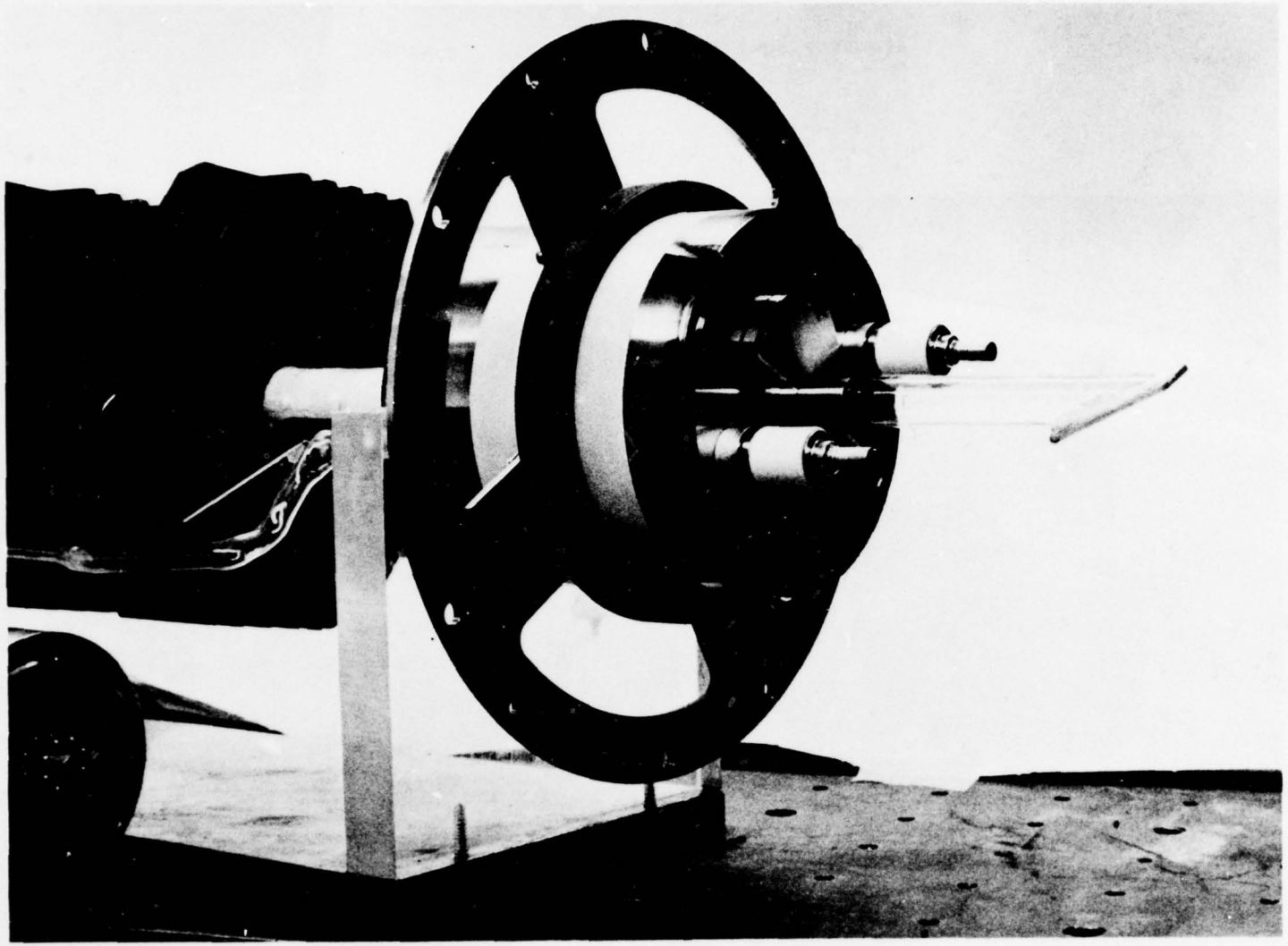

Figure 5. End Section, Laser Tube Assembly

2.3.2 Grating Tuner

The grating tuner assembly (674-0076) consists of the eight diffraction-grating modules (674-0074), a cylindrical mount (674-1348), and the scan motor and its housing (674-1349). The diffraction gratings are mounted in modules equally spaced at 45° increments around the circumference of the grating tuner housing. This is a 27-cm diameter x 12.3-cm wide aluminum cylindrical housing with eight machined mounting faces. An Inland d.c. motor, mounted inside a separate housing, is bolted to the rear face of the cylindrical housing. The scan mirror mount (674-1346) is attached to the portion of the motor shaft that extends into the grating tuner housing. Attached to the opposite end of the motor shaft is a flexible shaft coupling that connects to the shaft of the Teledyne-Gurley rotary encoder. The encoder is clamped to the rear wall of the motor housing.

The eight diffraction gratings used to tune the laser at eight independent wavelengths were obtained from PTR Optics Corp. These standard ML303 gratings were replicated on glass substrates and vacuum-coated with aluminum. The specifications for the ML303 gratings are:

Grooves/mm:	150
Blaze Wavelength:	10.6 μm
Angular Dispersion:	42Å /mrad
Relative Efficiency:	92% at 10.6 μm

The grating dispersion was selected to prevent simultaneous lasing at more than one transition and to provide easy rotational tuning.

The purpose of the Grating Module Assembly (674-0074) shown in Figure 6 is to provide adjustable rotation of the grating about axes of rotation both perpendicular and parallel to the ruled lines on the front surface of the grating. The grating module is a two-axis gimbaled mount that utilizes Bendix flexure pivots as gimbal supports. The torsional preloaded spring force of the pivots provides the reaction force necessary to maintain the gimbal tilt arm clamped to its adjustment screw.

Each grating is mounted in the inner gimbal at a nominal Littrow angle of 55° (10.92 μm). The inner gimbal rotates the grating about an axis parallel to its ruled lines. Laser tuning between 9.2 and 11.0 μm is accomplished by rotating the grating angle from 43.6° to 55° by one of the two adjustment screws in the outside fixed frame of the grating module.

The outer gimbal provides the required independent alignment of the grating about the axis perpendicular to the grating ruling. For lasing to occur, it is required that the outer gimbal be adjusted until the ruled lines are perpendicular to the optical axis of the laser.

The head of a 0.65-cm diameter socket-head screw has been bonded to the back surface of the grating. It is used to rotate the grating in its gimbaled mount. This rotation of the grating around the optical axis is necessary

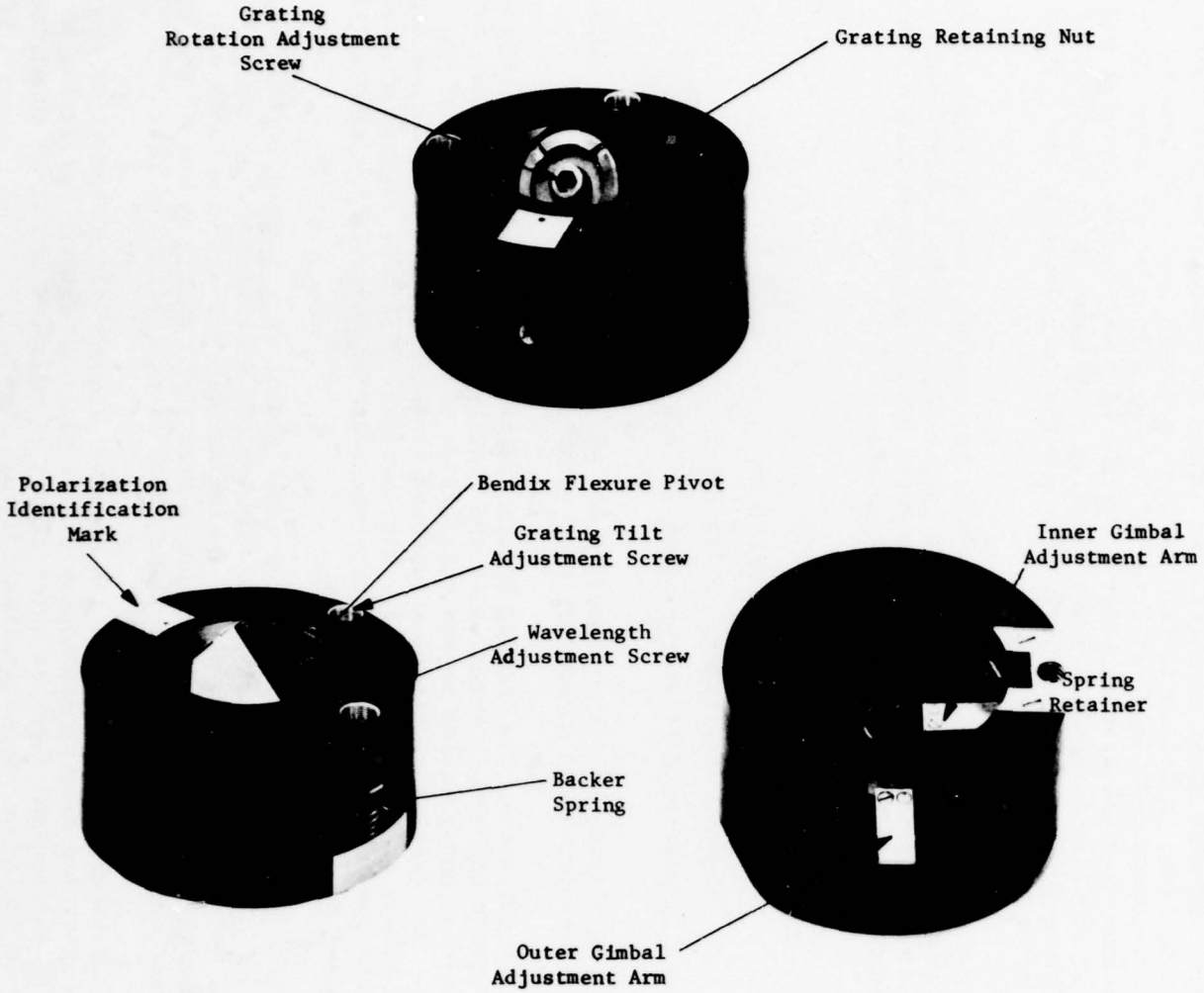

Figure 6. Grating Module Assembly

during initial grating prealignment to insure that the grating rulings are precisely parallel and perpendicular to the rotational axes of the grating module.

A detailed description of the grating prealignment and alignment procedure may be found in paragraph 4.4.1. No attempt should be made to tune the laser without carefully following these procedures. Over-adjustment of either gimbal axis will cause damage to the flexure pivots.

A d.c. motor was selected to drive the laser scan mirror and Teledyne-Gurley incremental encoder. The Inland model Y-1258-B motor may be operated at speeds ranging from several revolutions per second to well over 100 rps (see Figure 7). Precision duplex bearings limit radial shaft runout to less than 0.025 mm. The direction of rotation may be reversed by inverting the drive voltage polarity.

A Teledyne-Gurley Model 8635-1024-051 rotary incremental encoder is used to monitor the angular position of the rotating scan mirror to an absolute accuracy of ±1 arc-minute. The encoder is mounted to the end plate of the motor assembly with standard servo clamps. A flexible shaft coupling (Helical Products Model 5005-8-10) couples the encoder to the Inland scan motor. The encoder generates 1024 Hz square-wave per revolution along with a zero reference index pulse from a differential line driver.

2.3.3 Collimator Assembly

The collimator assembly contains the laser output coupling mirror, its mount (674-0083), and the optics required for beam expansion (674-1210). A 25-cm diameter mounting plate (674-1138) is bolted and pinned to the fore end housing. Mounted on this plate is the coupling mirror mount over which the collimator housing is bolted.

The 2.5X beam expander optics converts the output beam to a diameter of 1.7 cm with a full-angle beam divergence of approximately 2.5 mrad. The optics consist of two ZnSe elements having a nominal spacing of 52.15 mm. The smaller 16.7-mm diameter element, closest to the coupling mirror, is bonded to a machined seat in the collimator housing. The second larger element is bonded to an adjustable lens cell (674-1161) that threads into the front of the housing. The same threads are also used to secure the protective lens cap (674-1163).

The output coupling-mirror mount is similar in design to the eight grating mounts. The inner and outer gimbals are independently adjustable ±4° in a plane normal to the optical axis. Bendix flexure pivots keep the gimbal adjustment arms clamped against the two alignment screws located in the outer frame of the mount. Access to the screws can only be made by removing the collimator housing. During initial laser alignment, the mirror was aligned normal to the laser optical axis using the alignment HeNe laser. The eight gratings were then aligned to the mirror. The flexure mounts are sufficiently stiff to maintain mirror alignment for anticipated shock and vibration levels. Should it ever become necessary to adjust the coupling mirror, care should be taken not to damage the flexures by adjusting them beyond their ±4° limit.

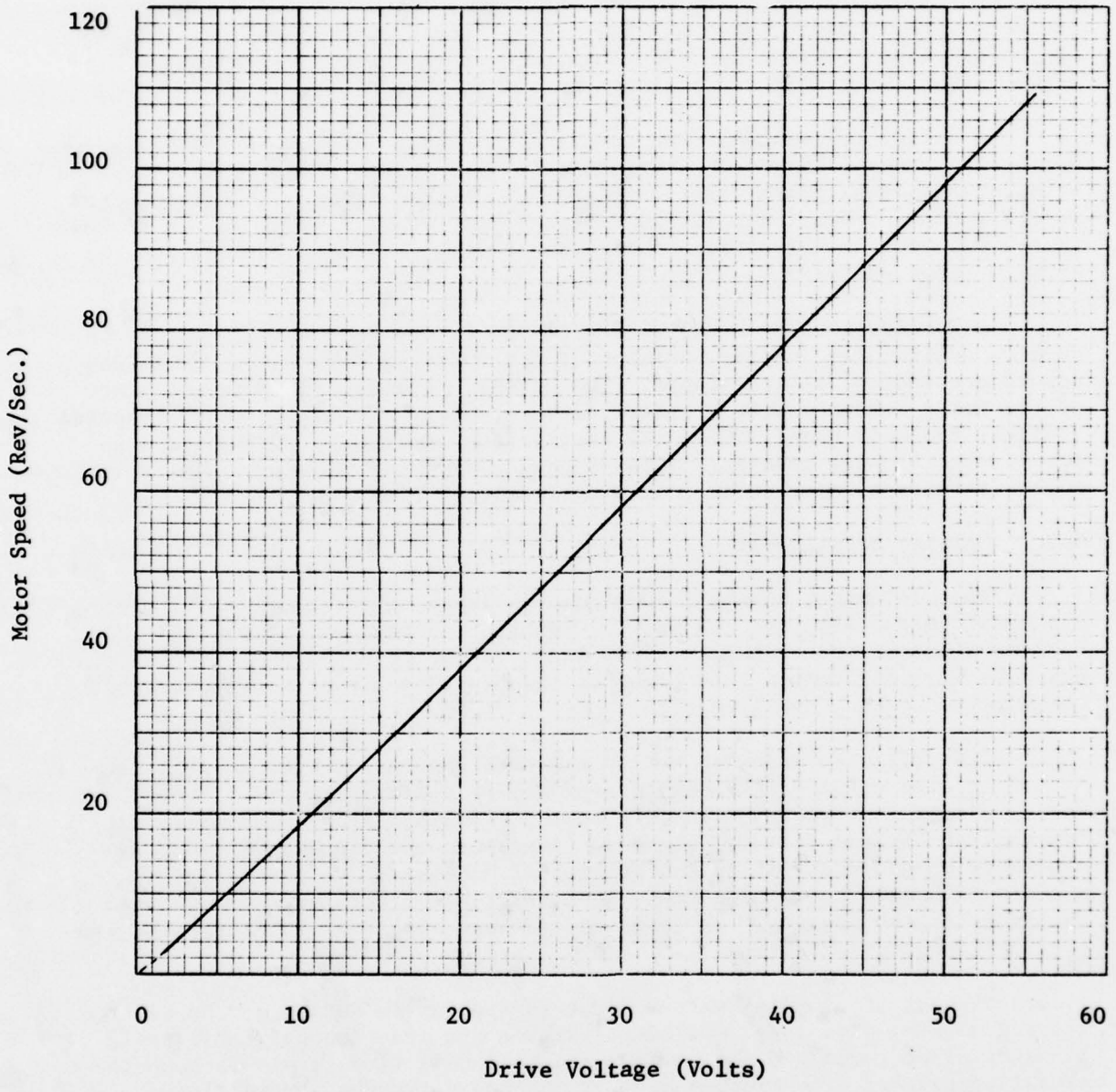

Figure 7. Scan Motor Speed Vs. Drive Voltage

2.3.4 Reference Detector

The reference detector is a Molectron P1-33 pyroelectric detector. A 3-mm diameter detector element and a wide-band FET operation preamplifier are housed in a TO-99 transistor package. A germanium window, anti-reflection coated at 10.6 microns, is mounted in the top of the can. The detector package is mounted in the reference detector mount (674-1374), which, in turn is mounted to the laser end housing (674-1166). In this position, the reference detector samples peak laser power by measuring the Brewster window reflection at the high-potential end of the laser tube assembly.

A 1-megohm resistor and a parallel 1-pf capacitor are used as feedback elements for the FET amplifier to provide approximately a 300 kHz signal bandwidth and a corresponding detector noise-equivalent-power of 3×10^{-7} w/Hz$^{1/2}$ (see Dwg. B 674-1374-E). Note that (as indicated on Dwg. B 674-1374-E) the FET operational amplifier offset and bandwidth control outputs are not connected to minimize stray lead capacity.

2.3.5 Alignment Telescope

A Redfield RM 6400 Target Scope, mounted to the side of the laser transmitter, is coaligned with the laser optical axis. The telescope's 16X magnification and 1.24° field-of-view assist in aligning the laser on distant targets.

Two micrometer style knobs may be used to adjust elevation and azimuth pointing in 1/4 minute-of-arc steps to an accuracy of ±2 seconds of arc. Parallax may be eliminated at any range from 15m to infinity. This is accomplished by setting the parallax setting on the objective bell to the range desired.

2.3.6 HeNe Alignment Laser

A 2.0-milliwatt HeNe laser may be used to align and visually point the laser transmitter at close ranges and was used during the initial alignment of the laser output coupling mirror and target telescope. The Hughes Model 3022H laser is mounted on the side of the laser tube assembly in precision "V" blocks. Its output beam is folded by an adjustable mirror located on the top of the grating housing. This fold directs the beam into the grating assembly where it strikes the laser scan mirror. With the scan motor turned off, the scan mirror may be manually positioned so that the HeNe beam passes directly through the laser tube assembly. The proper scan mirror angle may be located by observing the retroreflected beam, from the output coupling mirror, back at the output aperture of the HeNe laser.

Proper alignment of the HeNe laser may be checked by first visually inspecting that it is centrally located in each Brewster window and at the output side of the laser coupling mirror (collimator assembly removed). Next, the CO_2 laser and scan motor are turned on, and the CO_2 output beam is focused by an off-axis reflecting mirror. When heat-sensitive Thermofax paper is placed at the focus of the beam, its recorded thermal image should be at the same location as the HeNe image. This procedure is helpful in aligning the Optical Engineering CO_2 Laser Spectrum Analyzer used to identify and set the desired laser output wavelengths.

The HeNe beam divergence is 1.3 mradians, and a three-minute warmup is required for the laser to reach its 2 mwatt output power level. Angular drift is less than 0.03 mradians after a 15-minute warmup.

2.3.7 Laser Gas Mixture

Prior to introducing isotopic $C^{13}O^{16}_2$ to the laser, a conventional mixture of CO_2 -N_2 - He and Xe was used for gas optimization measurements. The roles of the additive gases are fairly well understood and are discussed extensively in open literature[2]. In the CO_2 - N_2 - He laser, population of the upper laser level is principally due to collision excitation of ground state CO_2 molecules by vibrationally excited N_2. Helium assists in more efficient relaxation of the lower CO_2 level. In sealed lasers, Xe is used to reduce the electron temperature of the plasma and retards CO_2 dissociation.

The work reported by Clark and Wada[3] was of particular value in establishing the optimum gas mixture. Since the active path length of the laser is only slightly longer than that utilized by Clark and Wada, we were able to compare results with a minimum of scaling. Thirty watts of CW laser output power was obtained at 10.6 μm with 20 mA of discharge current for the following gas mixture:

CO_2	2.6 torr
N_2	2.6 torr
He	11.0 torr
Xe	0.8 torr

These results compare favorably to the 28 watts of maximum power reported by Levine and DeMaria.

Gas mixing was accomplished with the filling/mixing station shown to the right of the laser tube assembly in Figure 8. It was found that considerable time was required after the addition of each new gas for it to diffuse uniformly throughout the laser and fill-manifold. A mixing reservoir was later added to reduce this diffusion time and to allow mixing at higher, more convenient monitoring pressures.

An experiment was performed to establish the optimum pressure for maximum output power. The pressure of the gas mixture was varied in steps from 28 to 12 torr, and a broad maximum was found at about 17 torr. All of the above measurements were made with a 2m radius-of-curvature output coupling mirror having 91% reflectivity at 10.6 μm. When a similar ZnSe mirror having a reflectivity of 85% was substituted, the laser output power dropped by 17%. From these results, the final system mirror was selected. A 3m radius-of-curvature mirror was coated by Perkin-Elmer that had 92.7% reflectivity at 10.1 microns and 90% reflectivity at 9.2 and 11.3 microns.

---

[2] A.K. Levine and A.J. DeMaria, Lasers: A Series of Advances, Vol. 3, Marcel Deker Inc., New York (1971).

[3] P.O. Clark and G.Y. Wada, "The Influence of Xenon on Sealed-off CO_2 Lasers," Journal of Quantum Electronics, QE-4, No. 5 (May 1968).

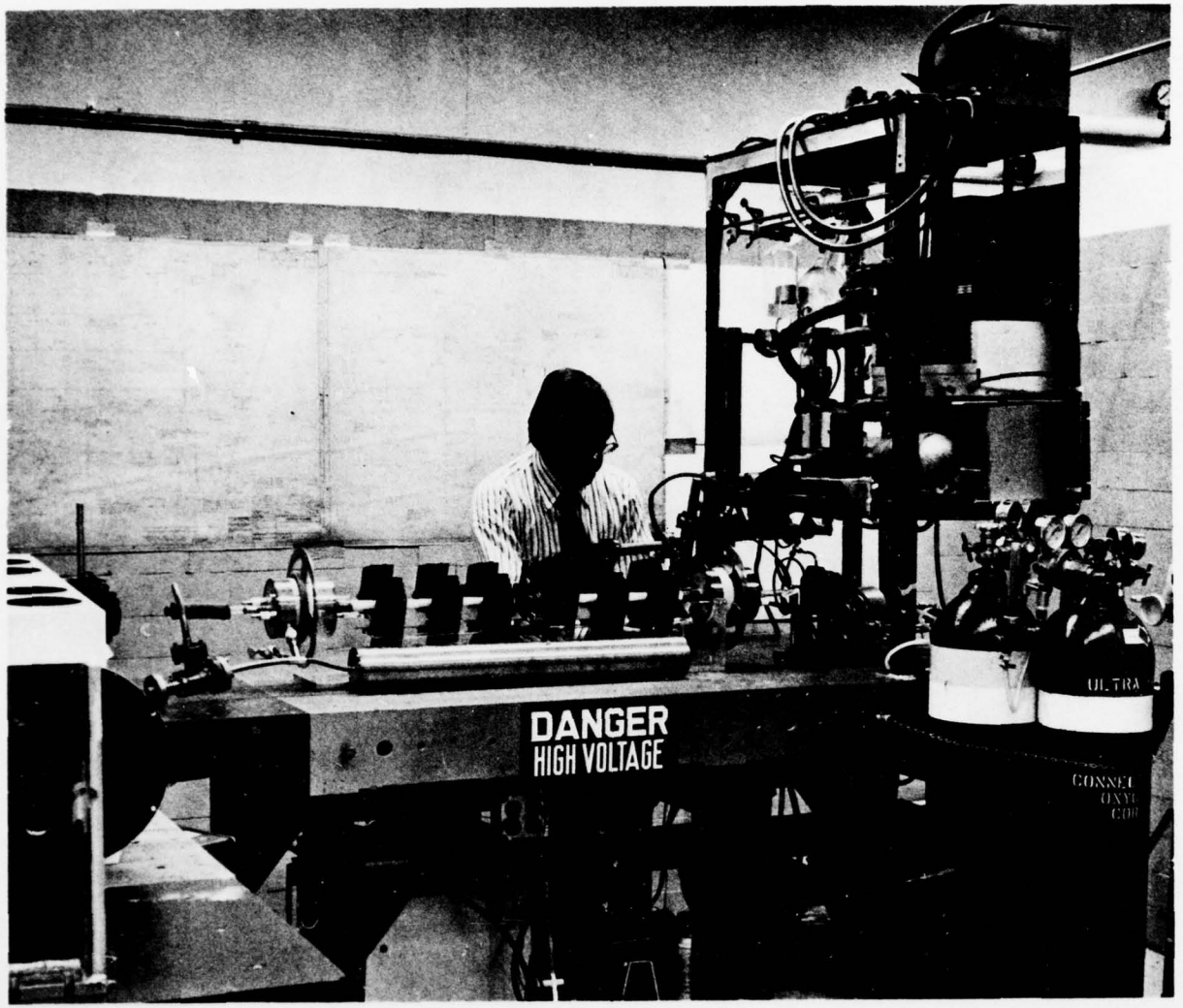

Figure 8. Laser Tube Assembly and Filling/Mixing Station

2.4 LASER RECEIVER

The laser receiver design was based upon providing a convenient but economical optical system for collecting and detecting laser radiation reflected/scattered from distant targets. The receiver shown in Figure 2 consists of an f/4.0, 127-cm Newtonian telescope, receiver optics, (PbSn)Te detector/dewar assembly, preamplifier and postamplifier. The receiver optics, detector/dewar assembly, and amplifiers are mounted on a common plate (674-1393), which is bolted to the side of the telescope at the exit port for the converging f/4.0 telescope beam. The receiver optics spectrally split the incoming energy into IR and visual components. IR energy is focused on the detector; the visual image is used to boresight the telescope.

2.4.1 Telescope

The basic telescope was purchased from Cave Optical Co. The 30-cm diameter primary and 7.6-cm diameter secondary mirror are supported in a 40-cm diameter fiberglass tube. The primary mirror mount was machined and rebuilt to provide precision mirror adjustment and more secure mounting. By machining the seat of the mirror mount flat, cork cushions were replaced with 0.03-cm thick mylar tape strips. New, more secure clamps and centering screws were also added along with finer thread adjustment screws and knobs.

This rework of the primary mirror mount reduces the possibility of mirror alignment shift during transport while providing a method for fine telescope pointing. Fine pointing is accomplished by means of the three adjustment knobs located at the back of the telescope. Because of the coalignment of the IR and visible images, the mirror may be adjusted until the desired IR target or reflector is positioned at the center of the cross-hair reticle viewed through the telescope eyepiece.

2.4.2 Receiver Optics

The receiver optics provides separate IR and visible images to allow simultaneous detection of laser energy with visual target viewing. Figure 9 is an optical diagram of the receiver optics located in the receiver housing with the detector/dewar assembly shown in Figure 10.

A dichroic beamsplitter, located just ahead of the f/4.0 telescope focus, reflects 92% of the incoming IR energy toward the detector/dewar but transmits directly visible light. The 5.4 x 1.6 cm beamsplitter is mounted in a C-shaped cradle (674-1367), which is pivoted to allow rotation of the beamsplitter about the optical axis in azimuth. The dichroic beamsplitter cradle is supported in a support tube (674-1393), which also holds the telescope eyepiece and cross-hair reticle. The support tube is mounted to the receiver optics baseplate (674-1393) by the tube support ring (674-1368). By loosening the nylon tipped setscrews located in the tube support ring, the support tube and dichroic beamsplitter may be rotated around the optical axis.

By rotating the support tube and C-shaped beamsplitter cradle, it is possible to coalign the IR and visible fields-of-view. This was accomplished using a large collimator and pinhole aperture placed in front of a blackbody source. The alignment and locking screws located in the C-shaped cradle insure a positive and permanent alignment.

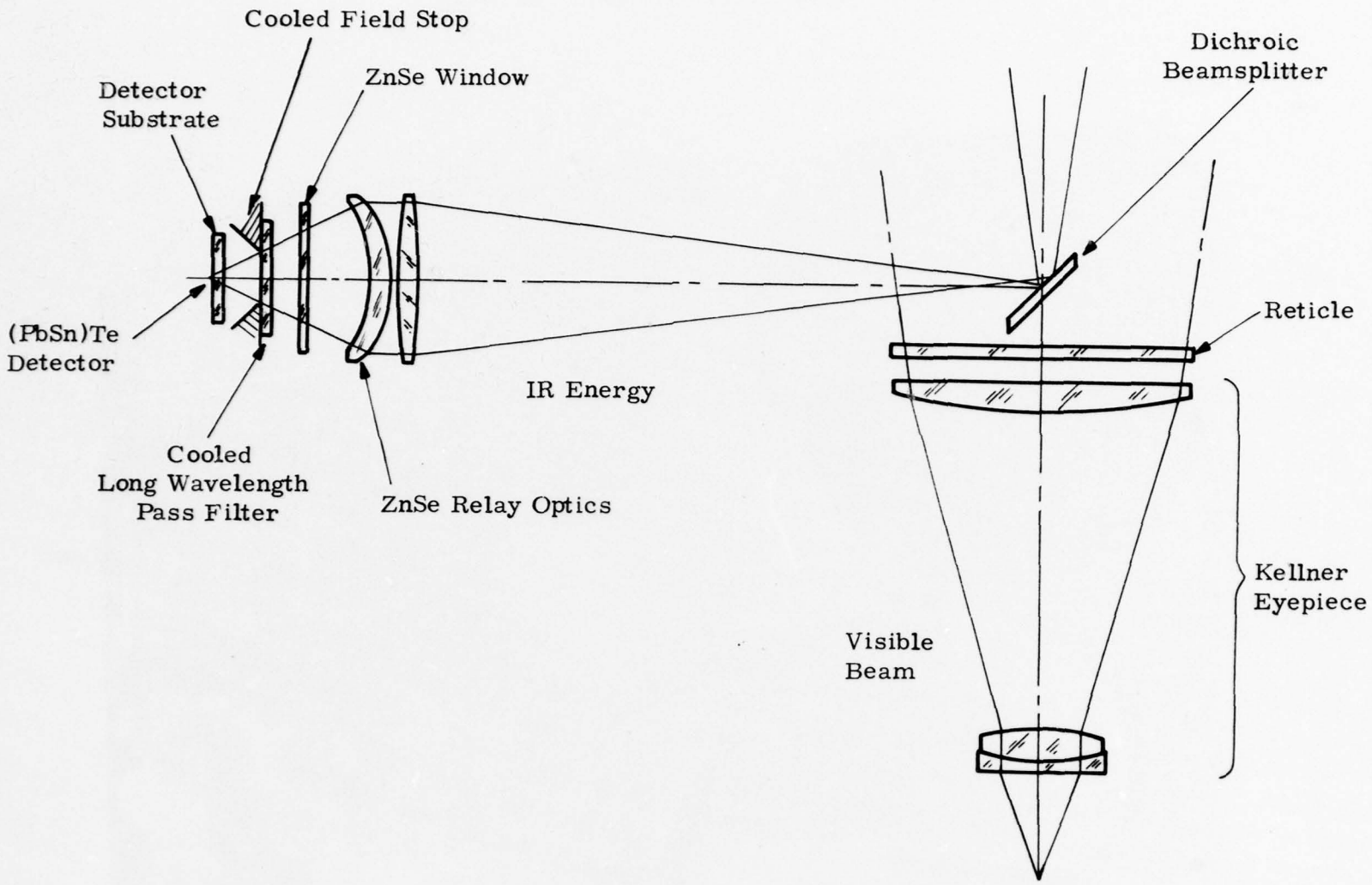

Figure 9. Optical Diagram - Receiver Optics

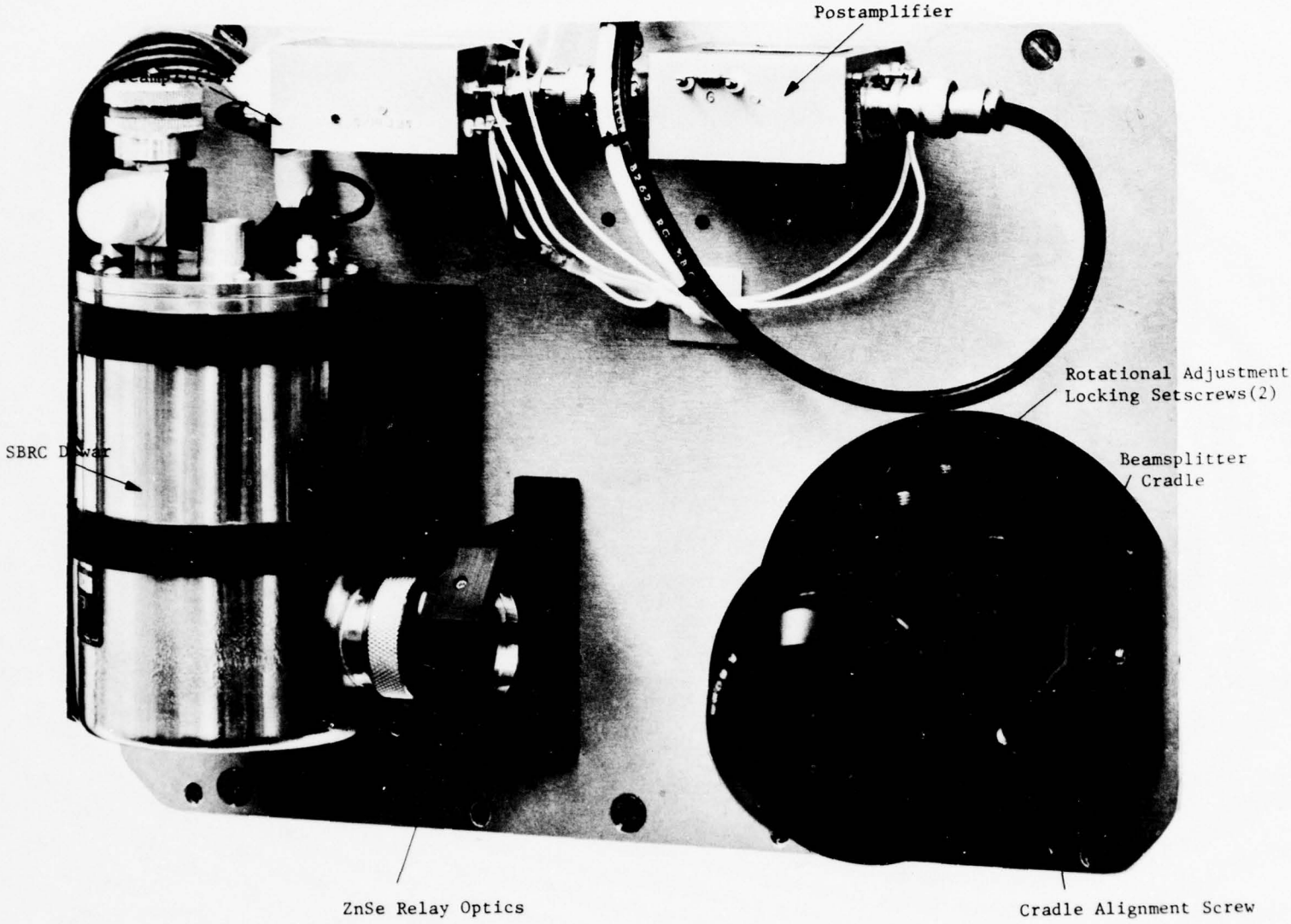

Figure 10. Laser Receiver Optics

A 60-mm focal length, 5-cm OD Kellner-type eyepiece is used to examine the visual image with a magnification of 21X. The 2.3° visible field-of-view is substantially larger than the 2.5 mradian (0.143°) IR field. A crosshair reticle is cemented just inside the front surface of the eyepiece placing it near the visible focus.

Infrared energy reflected from the front surface of the dichroic beamsplitter comes to focus just inside the support tube. The two-element IR relay lens (674-0213) transfers this focus to the detector plane located inside the stainless steel dewar. The relay lens magnifies the f/4.0 IR image by 3.175X so that the 1.0-mm diameter detector subtends the desired 2.5-mradian field-of-view. The optical path differences of the ZnSe dewar window and IR filter were included in the relay lens design.

The concave/convex element of the relay lens is cemented in a lens cell (674-1363). The second double-convex element is cemented in a second adjustable cell (674-1362), which threads into the first cell. The lens assembly is centered and locked in focus in a lens mount (674-1364). Both the lens element spacing and focus were adjusted during assembly and permanently locked. No further adjustment is necessary.

2.4.3 (PbSn)Te Detector and Dewar

A 1-mm diameter Schottky barrier (PbSn)Te detector is used to detect collected-laser energy. The detector substrate (674-1331) is epoxied to a copper detector mount (674-1333). This mount supports a cooled IR filter mount (674-1334) that also serves as a 77°K field stop. The IR filter is a long-pass coating deposited on a 9.8-mm diameter germanium substrate.

The detector and its mount assembly are housed in an SBRC Model No. 40742 side-looking stainless-steel dewar having a 2-mm thick ZnSe anti-reflection coated window (see Figure 11). The dewar has a 4-hour minimum hold time for LN_2 if its internal pressure is maintained at $1x10^{-4}$ torr or less. See section 3.4.2.2 for periodic pumping instructions.

The relative spectral response of the (PbSn)Te detector, with and without the cooled long-pass filter, is shown in Figure 12. Table 2 is a list of the more significant detector parameters.

2.5 SIGNAL PROCESSING ELECTRONICS

The major portion of the signal processor design was accomplished by Perkin-Elmer. However, final design, breadboarding, construction and testing of this unit was performed by the government when it became necessary to modify the contract scope to accommodate an expanded level of effort.

The processing electronics provide the interface between the laser and the dual-channel oscilloscope display. Inputs of grating position, reference signal, and return signal are utilized to generate a display showing the transmission of a gas at eight discrete absorption lines; 100% transmission is calibrated on-site to correspond to transmission in clean air. The processing may be subdivided into five general subsections as indicated below. Reference is made to the system electronics block diagram (674-0222).

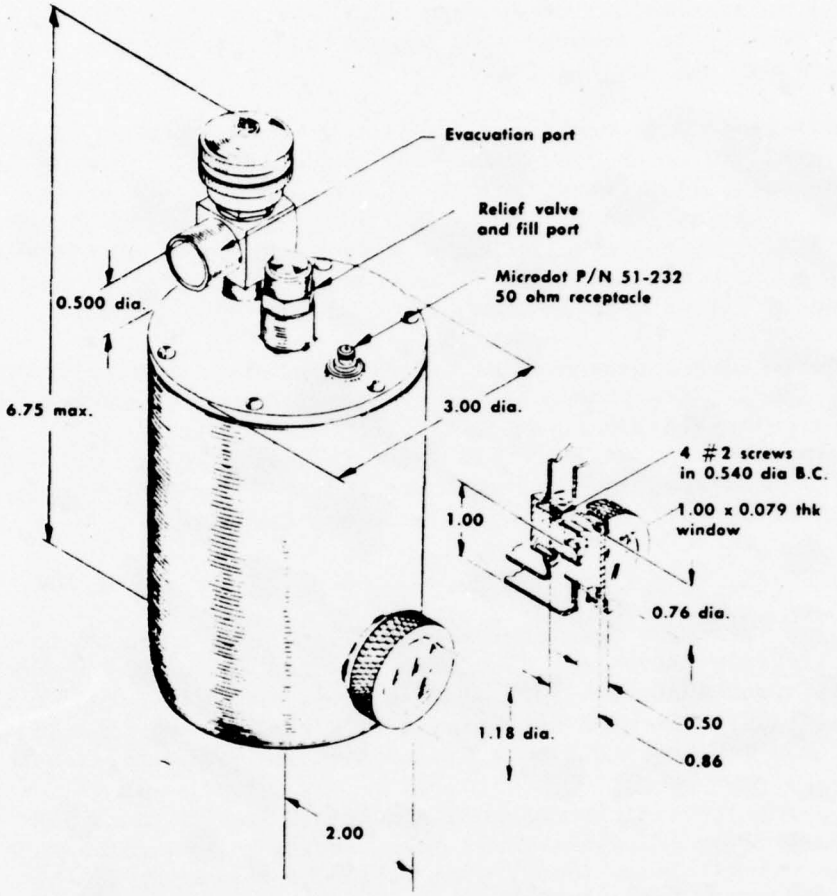

Figure 11. Model 40742 Stainless Steel Dewar

(1) Timing - A pulse from the shaft encoder clears the main counter between pulse 8 and pulse 1. This provides the timing circuits with the necessary scan mirror position information. As the laser rotates through the eight gratings, eight output pulses from the reference detector clock the main counter and create eight equally divided time frames within one 360° rotation of the laser scan mirror. Each time frame (1 through 8) has timing gates that provide appropriate gain scaling for filtering and remultiplexing the signal for display purposes.

(2) Reference Processing - The signal output of the pyroelectric reference detector is a.c.-coupled into a front panel control ("REF GAIN") and is presented to a bank of FET switches that are sequentially enabled and set the reference channel gain for each wavelength. This gain selection is provided to normalize gain across the eight wavelengths and to account for

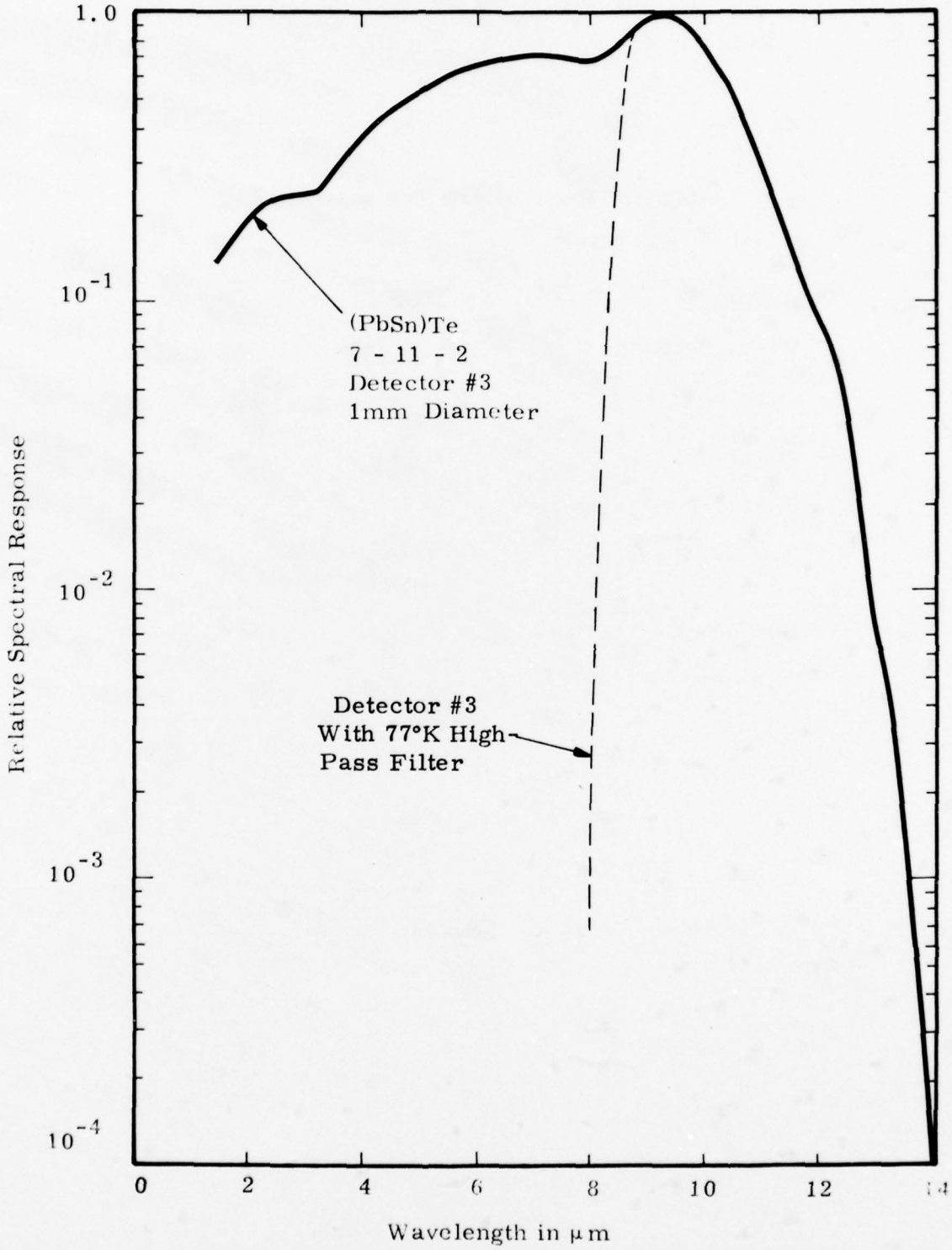

Figure 12. Relative Spectral Response (PbSn)Te Detector

TABLE 2. (PbSn)Te DETECTOR PARAMETERS

Parameter	Value
$D^*_{\lambda_p}$	5×10^{10} cm-Hz$^{\frac{1}{2}}$/W (300°K Background, 50° FOV)
Diameter:	1.0 mm
Operating Temperature:	77°K
Mode of Operation:	Photovoltaic (0 VDC bias)
Impedance:	40 Ω
Time constant:	<0.3 μsec
Noise:	0.6 nV/Hz$^{\frac{1}{2}}$

variations in laser power output. It is then gated, integrated, and held as one input to an analog divider. The reference signal is also presented to a comparator whose threshold is set above noise and whose purpose is to square-up the reference signal. The comparator output is used to initiate timing signals within each wavelength frame.

(3) Signal Processing - The return signal, following atmospheric absorption, is amplified in the receiver preamplifier and postamplifier (max. gain = 100db) and is a.c.-coupled via the front panel control ("SIG GAIN") to a bank of FET switches for sequential gain control in a manner analogous to the reference detector processing. Following further amplification, the signal is range-gated by setting front panel controls such that a range gate strobe encompasses the signal time slot. This process reduces background noise and enhances signal-to-noise ratio. The range-gated signal is then integrated and held for input to one side of an analog divider.

(4) Signal Ratioing - In order to accommodate random variations in laser output beyond those accommodated by the input FET gain-scaling networks, the signal is normalized to the reference signal by taking an analog ratio of the signal channel divided by the reference channel. This ratio may be set to any desired level for a ratio of one, but it is suggested that the output be 10 volts for equal 10-volt input signal amplitudes at the divider.

(5) Filtering - Due to the sequential time multiplexing of individual wavelength signals, coupled with the relatively long time constants of gas clouds, each wavelength signal is demultiplexed into a long time constant filter (τ = 1.6 seconds). Each filter channel consists of a peak holder followed by a single-pole active filter. The peak holder stretches the output level from the divider to cover the seven remaining time frames during which the input is disconnected.

(6) Display - The processor provides two output functions

a. Recorder signals

b. Oscilloscope signals

The recorder outputs are derived directly from the active filter outputs in each channel. For oscilloscope display purposes, the filter output signals are remultiplexed onto one line for display on scope channel 1. Additional signals are brought to scope channels 1 and 2 and scope sync to facilitate field calibration and operation.

3. TEST PROGRAM RESULTS

3.1 LASER TRANSMITTER

3.1.1 Grating Tuner Demonstration

The operation of the grating tuner was demonstrated with an Optical Engineering, Inc. CO_2 Laser Spectrum Analyzer. The wavelengths of tuned laser pulses were examined with this infrared grating spectroscope, which has a 3/4 meter dispersive distance and overall internal optical path length of 2.3 meters. The instrument output scale is calibrated in wavelength from 9.1 m to 11.3μm with the major $^{12}C^{16}O_2$ vibration-rotational lines identified.

An f/8.0 mirror was used to focus the laser output at the entrance slit of the spectrum analyzer. Instrument alignment was verified with thermal sensitive paper and the HeNe alignment laser. The output of the spectrum analyzer was monitored with a pyro-electric detector mounted to an exit slit designed to travel along the instrument's output scale. First, the laser reference detector was used to demonstrate that a laser pulse was emitted for each grating. The output of the reference detector was displayed on an oscilloscope that was synchronized with an index pulse from the rotary encoder. An adjustment to any one of the grating modules was then correlated with a change in amplitude to the corresponding laser pulse.

A single grating module was tuned over its total wavelength range (9.1μm to 11.0μm), and the amplitude and wavelength of each pulse observed were identified and recorded. Figure 13 is a typical spectral gain profile plotted for one of the eight gratings. Stable laser operation was observed on 54 rotational lines between 9.26 and 10.8μm for $^{12}C^{16}O_2$.

The output of the laser was also analyzed for several $^{13}C^{16}O_2$ gas mixtures. A total of 17 lines were observed in the R-branch of the 00°1-10°0 vibrational band. Attempts to achieve lasing in the 00°1 - 02°0 band were unsuccessful. This may possibly be due to the fact that the laser gain at ambient temperature was below threshold. Also, it is not known whether the gas mixture optimized for $^{12}C^{16}O_2$ is ideal for $^{13}C^{16}O_2$ laser operation. The scope of the contract did not permit further exploration of these possibilities.

3.1.2 Output Power Measurements

The laser tube assembly was first operated CW using an optical flat in place of a diffraction grating. A maximum power level of 30 watts was obtained for a ZnSe, 2m radius-of-curvature output coupling mirror having a reflectivity of 91% at 10.6 μm. When the laser was operated with a 3m radius-of-curvature mirror having a reflectivity of 85%, the CW power dropped 17%.

Next, the laser was operated with the scan mirror and a single, gold-coated optical flat. For the 91% output reflector mirror, a maximum of 60

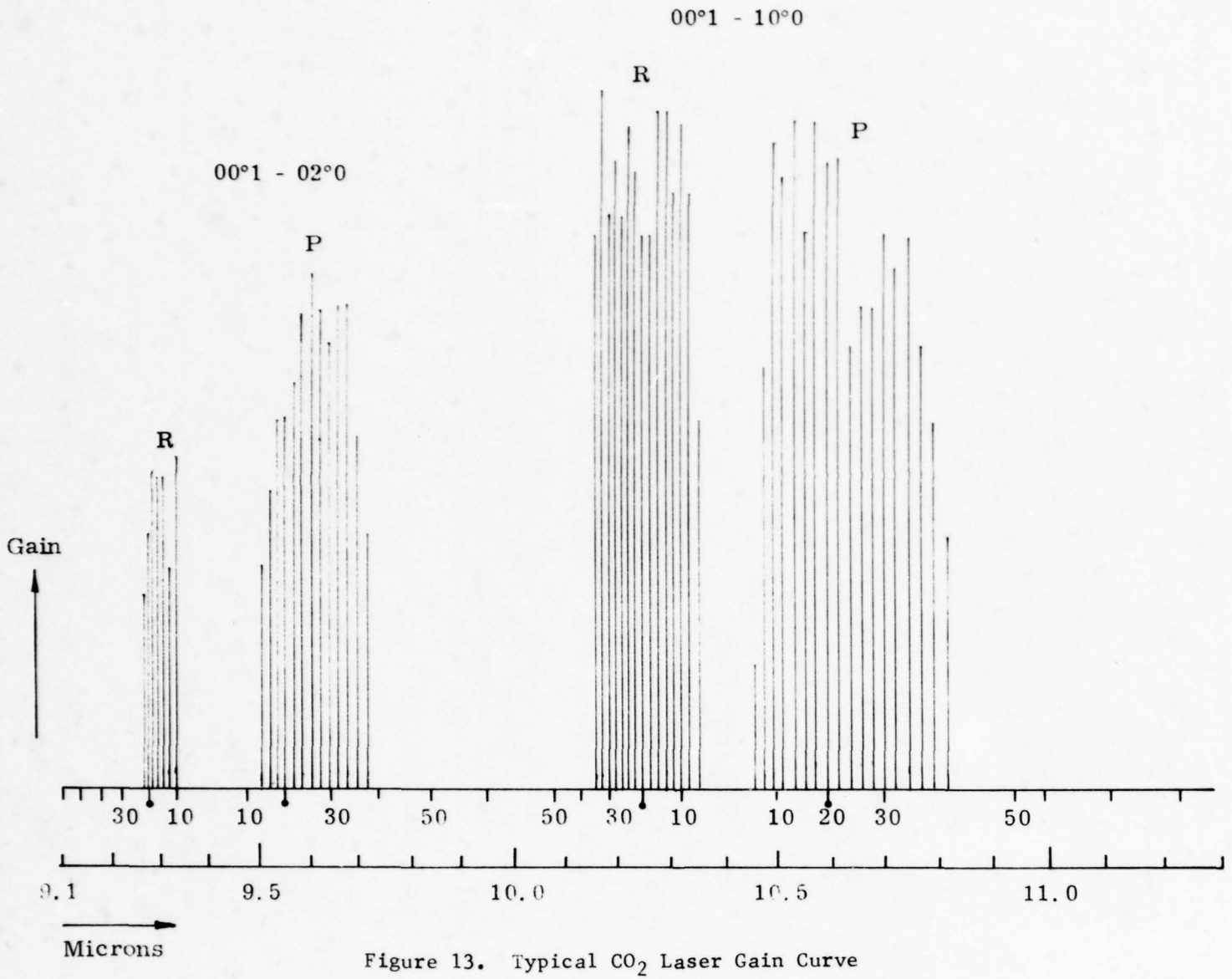

Figure 13. Typical CO_2 Laser Gain Curve

mwatts of average power was obtained in several lines simultaneously around 10.6 μm. The spectral reflectance of this coupling mirror dropped off very rapidly and was too low for operating with a grating at 9.2 and 11 μm. The laser was then operated with the mirror selected for tuned operation. This 3m radius-of-curvature mirror had a peak reflectivity of 92.7% at 10.1 μm that dropped to 90% at 9.2 and 11.3 μm as shown in Figure 14. A maximum of 45 mwatts average power was obtained for scanned operation with a flat mirror, indicating that the laser was undercoupled for the 92.6% mirror reflectivity at 10.6 μm. Again, several lines contributed to the total output power. Because of the decrease in line strength and mirror reflectivity at longer and shorter wavelengths, this undercoupling at 10.6 μm was not considered objectionable in light of the limited data available.

When the laser was later operated with a diffraction grating, pulse trains were observed having average power values as high as 25 mwatts on the stronger rotational lines. Identical power levels were obtained with both a Coherent Radiation Labs Model 201 power meter and a Scientech Model 362 unit. Estimates of peak power were limited by the uncertainty of the laser pulse width discussed in the next section. Laser power measurements for the $^{13}C^{16}O_2$ mixture were 30 to 40% lower than the corresponding CW and average pulse power levels.

3.1.3 Laser Pulse Width

The measurement of laser pulse width was limited by the 3 MHz bandwidth of the (PbSn)Te detector and its preamplifier. The laser pulse observed at the output of the preamplifier had a width of 380 nsecs at its half-amplitude points. Based upon work reported in reference 4, the actual pulse width is believed to range between 100 and 200 nsec.

Both the pulse width and amplitude were not a strong function of rotational speed between 20 and 200 Hz. It appears that the dynamics of the laser rather than the alignment time of the mirror established the pulse duration of the laser. Similar results were reported and discussed in reference 5.

3.2 LASER RECEIVER

Noise equivalent power measurements were made to establish receiver sensitivity to blackbody radiation between 9 and 11 μm. An Electro-Optics Inc. radiation source and square wave chopper were used to provide a 600°C, 0.127-cm diameter, chopped, blackbody source. The blackbody radiation was collimated by placing the source aperture at the 457-cm focus of an f/16 off-axis parabola. The receiver was then aligned to the optical axis of the collimator, and its output signal and noise were recorded using a Tektronix oscilloscope and camera. The average NEP of the receiver was found to be 3.4×10^{-8} watts in a 0.5-MHz bandwidth for radiation in the 9- to 11-μm spectral region.

---

[4] A.K. Levine, Lasers, A series of Advances, Dekker, Inc., New York, Vol. II (1968) and Vol. III (1969)

[5] D.C. Smith, "Q-Switched CO_2 Laser", IEEE J. Quantum Electronics, p. 291 (June 1969)

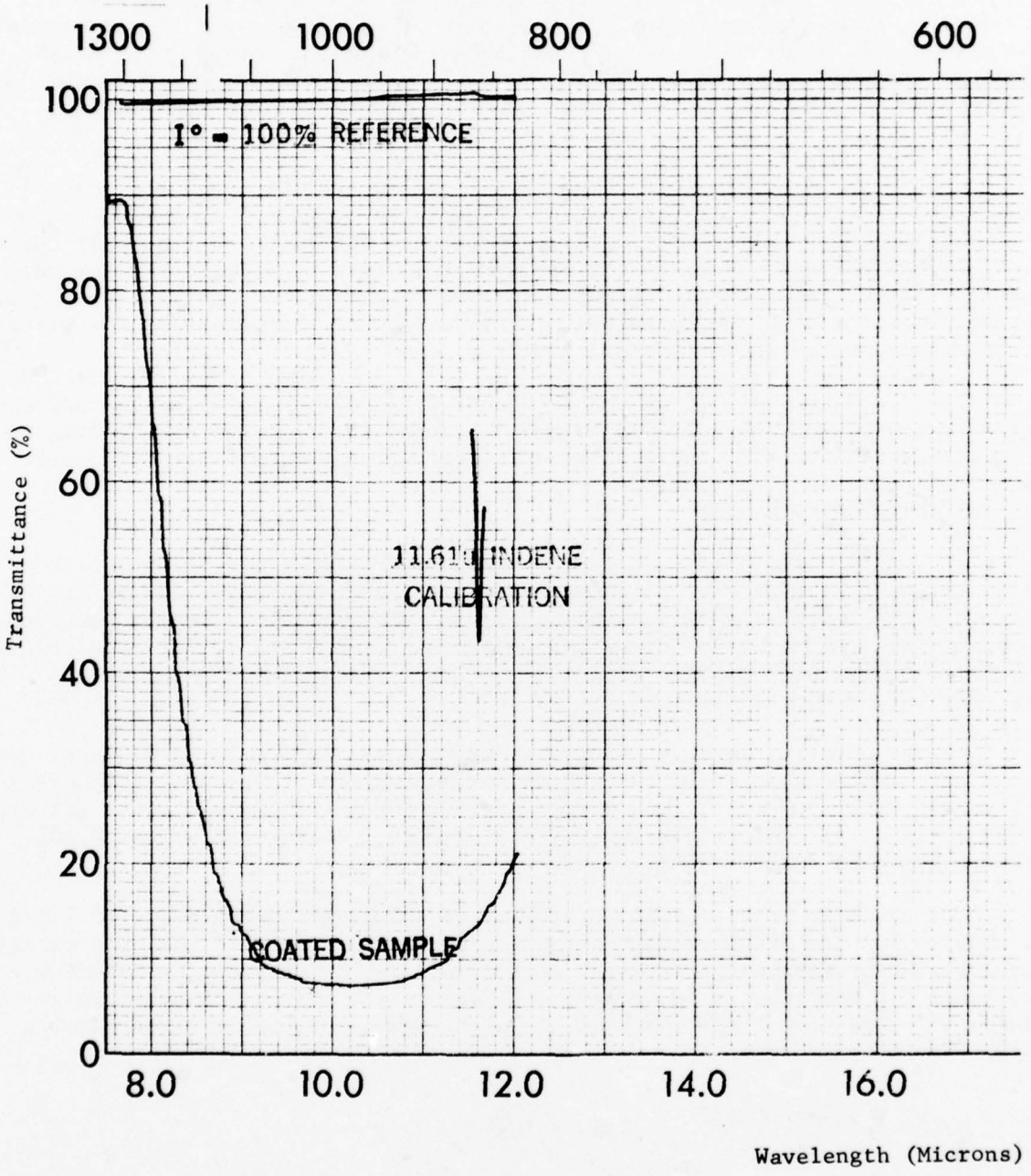

Figure 14. Spectral Reflectance 3-M Radius of Curvature Mirror

A field of view plot of the receiver, shown in Figure 15, was made by rotating the telescope in the collimated beam. A theodolite and mirror mounted to the telescope mount were used to establish telescope pointing. The slight nonsymmetry of the curve is due to the fact that the 1-mm diameter detector element establishes the receiver field-of-view. Variations in sensitivity across the element cause some curve distortion.

The infrared and visible telescope channels were aligned using the collimator and blackbody radiation source. First, the telescope tube was aligned to the optical axis of the collimator by centering the image of the small aperture of the blackbody source on the cross-hair reticle viewed through the telescope eyepiece. The dichroic beamsplitter was then adjusted and locked in rotation and tilt for peak output signal. This adjustment was made with the primary mirror firmly locked in its nominal position.

The focus and spacing of the 2-element ZnSe relay lens were also adjusted for maximum output signal. Since small changes in its focus and spacing do not appreciably affect signal amplitude, no future adjustments are necessary.

3.3 INTEGRATED SYSTEM TEST

A system performance test was performed at Perkin-Elmer to establish the laser system sensitivity to compare it with the design objective of the contract. The laser transmitter and telescope receiver were setup on the roof of one of Perkin-Elmer's buildings and were aimed at a black target at a range of 200m. The target consisted of a 1.2 m x 1.2 m panel of 6.35 mm plywood painted with 3-M Nextel Black Velvet paint.

If the normal reflectivity of the paint is assumed to be 2% or less, the results of the test indicated that the laser system met or exceeded the design goal sensitivity: "detect within 5 seconds a differential absorption of 10% with a 5 to 1 signal-to-noise ratio when operating with a diffuse target of 0.001 reflectivity at a range of 1000 meters".

For the stronger laser lines, a peak signal-to-rms-noise ratio of 7.5 to 1 was observed at the 3-MHz output of the video preamplifier. If the time constant of the signal processing integrating filter is set at 1.67 seconds, 95% of the amplitude of a step change in differential absorption will be observed in 5 seconds (3_σ-response). The observed signal-to-noise ratio in a corresponding 0.1-Hz bandwidth is equal to:

$$S/N = 7.5\left(\frac{3\times10^6}{0.1}\right)^{1/2} = 4.11 \times 10^4$$

To scale the observed signal to noise ratio to a 1-km test range, a 0.1% reflector, and 10% change in absorption, it is necessary to reduce the above S/N value by factors of 25.5, 20, and 10, respectively.

$$S/N \begin{cases} R = 1 \text{ km} \\ \rho = 0.001 \\ \gamma = 0.1 \\ f = 0.1 \text{ Hz} \end{cases} = \frac{4.11 \times 10^4}{25.5 \times 20 \times 10} = 8.1$$

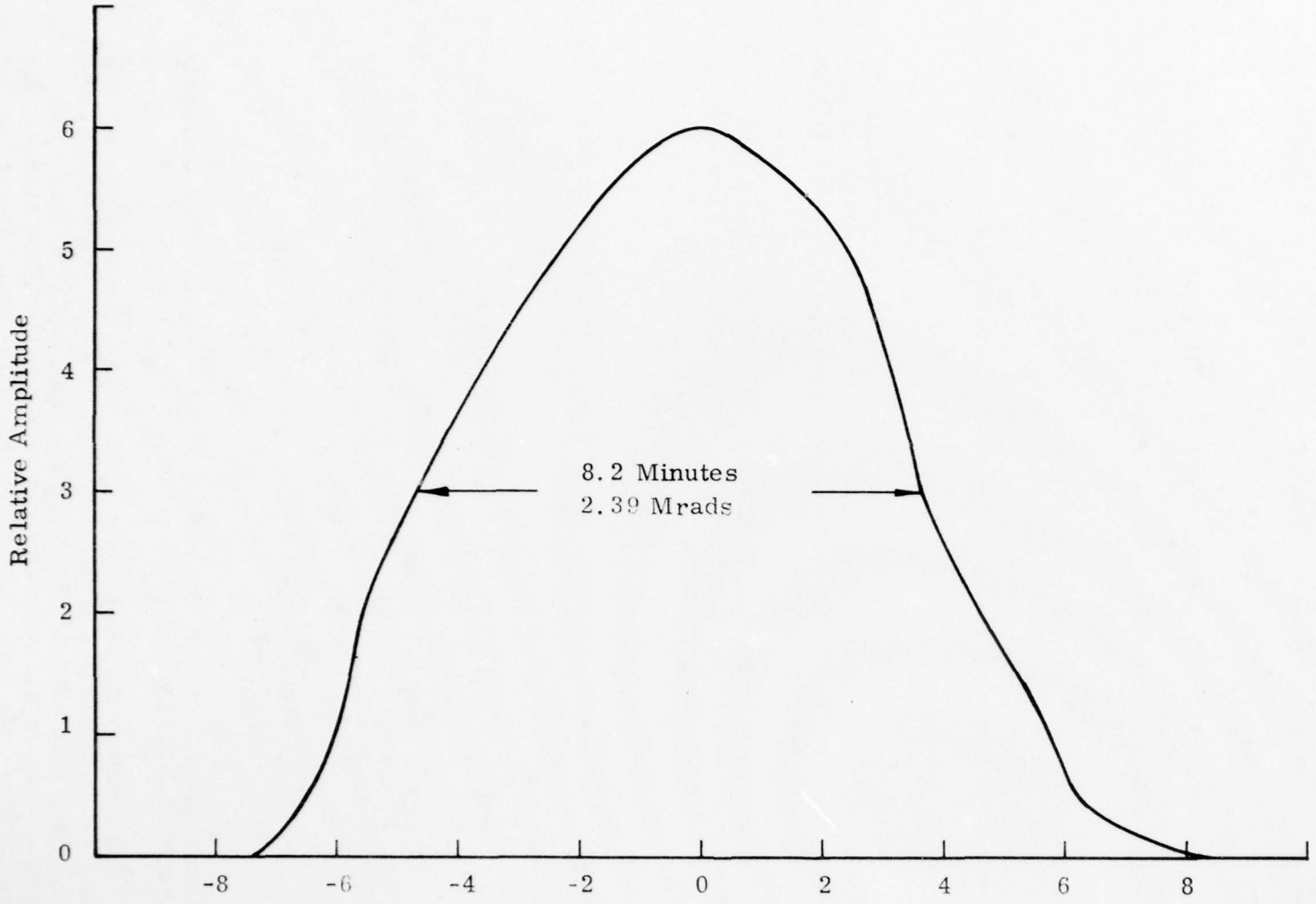

Figure 15. Field of View of Laser Receiver

3.4 RANGE SAFETY CONSIDERATIONS

Both the high voltage required to operate the laser and the moderately high-power laser beam represent hazards to personnel operating the laser system.

3.4.1 High Voltage Safety

The high voltage required to operate the laser poses a severe threat to personnel operating the laser unless a strict safety procedure is followed. The Hippotronics high-voltage power supply is capable of delivering 40k volts at 25 mA, which could cause a fatal shock. All personnel who expect to come in contact with the laser either in the laboratory or on the range should thoroughly review the detailed operating instructions described in the Hippotronics Operator's Manual for the Model 840-25 High Voltage Power Supply. In addition, the safety precautions and procedures found in paragraph 6.3.1 of the operation and maintenance instructions section must be followed at all times.

3.4.2 Laser Eye Safety

The laser transmitter radiates a moderately high-power beam that could be hazardous to operating personnel. The fact that radiation at wavelengths in the vicinity of 10 microns cannot be seen by the eye makes it especially imperative that precautions be taken.

According to radiation limits published by the American National Standards Institute, Standard Committee on Laser Safety, the allowable pulse exposure at 10.6 microns is given by;

$$E_p = 0.56T^{1/4}$$

where t is the laser pulse width in seconds. For a 0.2 microsecond pulse, the permissible pulse energy density is:

$$E_p = 0.56(2 \times 10^{-7})^{1/4} = 1.2 \times 10^{-2} \text{ J/cm}^2$$

The energy density level per pulse in the direct (uncollimated) beam of the laser is equal to the total energy per pulse divided by the cross-sectional area of the beam, or

$$E_L = \frac{2000 \text{ watts} \times 2 \times 10^{-7} \text{ sec}}{\frac{\pi}{4}(0.5)^2} = 2 \times 10^{-3} \text{ J/cm}^2$$

Since this level is 17% of the allowable pulse energy, there is little danger to the eye from a single pulse.

The commonly accepted level of CW radiation allowed at the eyes is 0.1 watt/cm^2 for a wavelength of 10.6 microns. The laser transmits 800, 0.2 microsecond pulses each second. The average output power of this pulse train is 0.32 watt, assuming all pulses have a peak power of 2000 kwatts. For the 0.5-cm diameter beam (uncollimated), the average power density at the output of the laser is

$$\frac{0.32}{\frac{\pi}{4}(0.5)^2} = 1.63 \text{ watts/cm}^2$$

The power density level in the direct beam of the laser is equal to or less than

$$H = \frac{Q}{(a + r\phi)^2}$$

where:

H = radiant exposure at range, r (watts/cm^2)

Q = average power at the laser output (watts)

r = range (cm)

a = beam diameter (cm)

ϕ = beam divergence (radians)

Substituting into the above equation, it is found that the average power in the direct beam is attenuated to the 0.1 W/cm^2 allowable level at a range of approximately 4 meters.

Based upon these calculations, safety procedures must be employed during laser operation. Eye protection devices (goggles) are required to be worn by all personnel within a distance of 15 meters of the operating laser. (This value includes a margin of safety.) In addition, accidental reflections of the main beam should be avoided as an added precaution. When the laser is operated with the 2.5X beam expander, the value of H at the laser output is reduced from 1.63 watts to 0.26 watt, or to a value 2.6 times the accepted safe limit.

4. OPERATION AND MAINTENANCE INSTRUCTIONS

4.1 INSTALLATION AND POWER REQUIREMENTS

The laser transmitter, receiver, and control/display console compose a self-contained system requiring only 20 amperes of 115 VAC single-phase power for operation. To aid in boresighting the laser transmitter and receiver, it is desirable to mount both units on a common flat surface such as a truck bed or laboratory table. When not in operation, the system should be protected from rain and windblown dirt and dust.

4.2 PARTS RECEIVED

The following list of parts and materials were delivered with the laser system to support and maintain its operation.

1 - Hughes 3590H laser power supply

1 - Black test target (1.2 x 1.2 m)

1 - Diffuse aluminum target (1.2 x 1.2 m)

1 - Grating alignment tool

1 - Grating alignment fixture

1 - Grating alignment wrench

1 - 2m, R of C, ZnSe 91% plano/concave mirror

1 - 5m, R of C, ZnSe 93% plano/concave mirror

4 - Boxes of spare hardware

4.3 SYSTEM OPERATION

4.3.1 Safety Precautions

The high voltage required to operate the laser is a serious threat to all operating personnel. All personnel who come in contact with the laser should be familiar with the procedures given below and in the Hippotronics Operators Manual for the Model 840-25 High Voltage Power Supply. Laser safety goggles must be worn by all personnel within a 50 ft. radius of the operating laser.

4.3.2 Startup/Shutdown Procedure

The first part of the startup procedure is to properly connect and verify the high-voltage power supply electrodes and safety grounds.

a. Check that the HV power supply ground lead (high-voltage return) is connected to the safety ground of the 115 VAC power source using an ohm-meter.

b. Connect a ground bus from the laser housing to the safety ground of 115 VAC power source; verify grounding using an ohm-meter.

c. Connect the power supply ground (high-voltage return) to the low-voltage laser electrode. This connection is made by passing the lead through the rubber grommet located in the end-housing at the output end of the laser. This connection should be verified by observing proper insertion of the banana jack in the low-voltage electrode housing through the Brewster window access port. Verify this connection using an ohm-meter.

d. Connect the high-voltage lead to the high-voltage electrode. This connection is made by passing the high-voltage lead through the rubber gasket located in the end-housing next to the motor/grating assembly. This connection should be verified by observing proper insertion of the banana jack in the high-voltage electrode housing through the Brewster window access port. Care should be taken to prevent any exposed portion of the high-voltage lead from coming in contact with the end housing or laser tube assembly.

e. Verify that the load bank attached to the back of the HV power supply is completely shielded and independently grounded to the safety ground of the 115 VAC power source.

WARNING

Do not turn on High Voltage until scan motor is activated. CW laser operation will damage gratings and scan mirror.

The laser system may now be safely turned on using the following procedure:

a. Check that all operating personnel are wearing safety goggles and that an area 15 m from the laser is restricted to all other personnel.

b. Place the circuit breaker on the laser control panel of the control/display console to its POWER ON position.

c. Depress the PROCESS ON and SCAN ON pushbutton switches on the laser control panel.

d. Check the rotational speed of the scan motor by observing the SCAN RATE meter (tachometer) on the laser control panel.

e. Adjust the SCAN CONTROL knob on the laser control panel until the SCAN RATE meter reads 6,000 rpm.

f. Turn the Hippotronics High Voltage Power Supply AC POWER switch to its ON position and its CURRENT RANGE switch to the HIGH position.

g. Check that the HV supply POLARITY switch is set at POS.

h. Set the RAISE VOLTAGE knob to O-Volts at its extreme counterclockwise position and depress the HIGH VOLTAGE-ON switch.

i. Slowly rotate the RAISE VOLTAGE knob until the high-voltage meter reads 18 kvolts, then rapidly increase the voltage to 25 kvolts. An 8 to 15 m amp current reading will be observed on the high-voltage supply current meter.

j. Raise or lower the high voltage until a value of 10 m amp is indicated on the current meter.

k. Check for laser operation by observing the reference detector output on scope channel 1 with the scope selector switch to GAIN SET. Scope channel 1 will show the signal return.

l. Adjust the signal and reference gain controls for nominal signal levels and adjust the band of FET gain switches to minimize amplitude variations from wavelength to wavelength.

m. Set scope selector switch to position RANGE GATE. Scope channel 1 will show the signal; channel 2 will show the range gate. Adjust the range and gate width controls until the range gate just straddles the signal.

n. Set scope selector switch to position RATIO/BALANCE. Scope channel 1 will show the signal input to the divider; channel 2 will show the reference input to the divider. Readjust the signal and reference gain controls to equal 10 volt signals.

o. Set scope selector switch to position T/R. Scope channel 1 will display the filtered transmittance signal, and channel 2 will display the unfiltered transmittance signal. Adjust each filter-channel gain potentiometer until channel 1 shows a straight line of 10 volts amplitude (corresponding to 100% transmission in clear air).

In operation, the scope selector switch should be set to position T/R. Any signal output less than 10 volts will indicate absorption at its corresponding wavelength.

4.4 GRATING ALIGNMENT PROCEDURE

4.4.1 Grating Pre-Alignment

As discussed in Section 2.3.2, the ruled grating lines are required to be aligned precisely parallel and perpendicular to the rotational axis of the grating module. In addition, the grating module itself must be mounted to the grating tuner housing in the position that causes the electric polarization vector of the laser beam to be perpendicular to the grating rulings.

The following procedure is required to align a grating and its module should they be disassembled.

a. Place the grating in the inner gimbal of the grating module, taking precautions not to damage its front surface.

b. Place the 2.5 cm diameter brass retaining washer on the back of the grating, and lightly secure the grating retaining nut (674-1173).

c. Bolt the grating module assembly to the back surface of the grating alignment jig (674-1205), and mount the jig on an optical surface plate.

d. Mount a low-power HeNe laser on the surface plate in front of the alignment jig, and direct its beam onto the center of the grating.

e. Place an optical flat on the front surface of the grating alignment jig to reflect the HeNe laser beam back on itself, and adjust the laser to center the return beam on the laser output aperture.

f. Using an Allen wrench, slowly rotate the grating until a series of spots (corresponding to the multiple grating orders) are projected vertically on a white screen or wall.

g. Carefully rock the inner gimbal of the grating module back and forth. The projected laser spots will travel up and down the screen with a slight sideways motion. If the sideways motion is to the right, make a slight counterclockwise adjustment of the grating; if to the left, make a clockwise adjustment.

h. Repeat step g until the projected spots travel precisely vertically without observable side motion.

i. Secure the grating retaining nut and repeat step e to check that the alignment has not shifted.

j. Bolt the grating module to the grating tuner housing in the position where the machined flat on the top surface

of its outer frame lines up with the index mark located next to the grating module mounting seat.

NOTE

The index marks next to the grating module mounting seats on the grating tuner housing indicate the direction of the laser beam electric polarization vector. This vector rotates 45° between adjacent grating module mounting locations.

4.4.2 Grating Tuning

After the grating has been prealigned and its module has been bolted to the grating tuner housing, no further rotational adjustments of the grating are necessary. Final alignment of the grating is made with the laser operating. The tilt alignment screw is used to align the grating perpendicular to the optical axis of the laser while the wavelength adjustment screw selects the desired operating wavelength (see Figure 6). During the pre-alignment of the grating, the tilt adjustment was used to set the outer gimbal and grating perpendicular to the optical axis of the HeNe laser (autocollimation step). This outer gimbal rotates the grating around the axis parallel to its rulings. When the grating module is transferred from the alignment jig to the grating housing, its tilt alignment will be very close to that required for maximum laser output. The following procedure should be followed to tune the laser to a particular wavelength.

a. Turn on the laser following the turn-on instructions detailed in paragraph 4.3.2.

b. Turn on the HeNe alignment laser.

c. Focus the laser output on the entrance slit of the CO_2 Laser Spectrum Analyzer.

d. Reduce the scan motor supply voltage until a 10-Hz bright red flicker is observed on or near the entrance slit to the spectrum analyzer.

e. Verify the location of the infrared focus using thermal-sensitive paper, and align the CO_2 Laser Spectrum Analyzer per its operating instruction manual for an external detector.

CAUTION

Do not operate scan motor at speeds less than 10 Hz. CW laser operation will damage gratings and scan mirror.

f. Display the output of the reference detector on the console oscilloscope and identify the position where the pulse will occur for the grating under adjustment.

g. Slowly adjust the wavelength adjustment screw until a pulse is observed on the oscilloscope. If the tilt adjustment is near its optimum alignment point, a pulse will quickly be found. If no pulses are observed, systematically adjust the tilt alignment screw ± 1/2 turn from its initial position. After each tilt axis adjustment, search for laser pulses by adjusting the wavelength alignment screw ± 1 turn.

h. When lasing occurs from the grating under adjustment, carefully adjust the tilt axis screw to obtain peak pulse power.

i. Use the spectrum analyzer to identify the wavelength of the pulse just adjusted. To verify that the pulse being observed corresponds to the grating being adjusted, rotate the wavelength adjustment screw a small fraction of a turn. If the observed pulse disappears, the proper pulse has been identified, and its wavelength may be read directly from the spectrum analyzer calibration scale at the location of the exit slit.

The above procedure may be used to peak the output and set the wavelength of each of the eight gratings.

4.5 FIELD MAINTENANCE

No regular or scheduled maintenance is required for the laser sensor system. The scan motor bearings are self-lubricated and shielded for the life of the motor. Occasional cleaning of the transmitter and receiver optics may be desirable should the units be operated or exposed in a high dust environment without their protective covers.

4.5.1 Cleaning Receiver Optics

The performance of the telescope and receiver IR and visible optics are remarkably tolerant to an unavoidable level of dust that may accumulate over a period of time. Dust from the telescope primary and receiver optics can be removed safely by blowing dry air or nitrogen across the elements. Omit Plus, distributed by Century Laboratories, Glencoe, Ill., is a convenient non-liquid lint and dust remover. Should any optical element become contaminated by grease or finger prints due to mishandling, the following cleaning procedure is recommended to be followed with extreme caution.

WARNING

This procedure must not be used to clean laser transmitter optical elements.

a. Wash hands thoroughly to ensure that excess skin oils are removed, then put on plastic gloves or finger shields.

b. With a dry air or nitrogen source, blow all particles from the surface to be cleaned.

c. Fold a clean piece of lens tissue twice and wrap smoothly around the index finger, being careful not to touch the front surface. (Always form lens tissue into smooth pad.)

d. Moisten the pad of lens tissue with a suitable detergent--1 part Orvus (Proctor and Gamble, Cincinnati, Ohio) to 9 parts water--and gently swab optical surface using a smooth continuous motion working toward the edge.

e. Gently wipe optical surface with a clean, dry lens tissue. Use long sweeping strokes, avoiding a back-and-forth motion.

f. Dampen a pad of lens tissue with methyl alcohol and gently swab optical surface using a smooth continuous motion, working toward the edge and rolling the index finger so as to continuously contact a new portion of the lens tissue. Repeat, as necessary, until all traces of grease are removed.

g. Gently wipe optical surface with a clean, dry lens tissue.

h. Moisten a pad of lens tissue with acetone and gently swab the surface using a smooth continuous motion, working towards the edge and rolling the index finger so as to continuously contact a new portion of the lens tissue.

i. Blow any remaining dust or lint from the surface using clean, dry air or nitrogen.

4.5.2 Cleaning Laser Optics

The laser optics should be kept free from significant levels of dust accumulation. When necessary, dry air or nitrogen can be safely used to clean the Brewster windows, scan mirror, gratings, and beam expander optical elements. No other cleaning procedure is recommended or considered necessary for the diffraction gratings. Occasional cleaning of the Brewster windows, scan mirror, and front surface of beam-expander optics with acetone may be desirable. This cleaning should be limited, and the following procedure should be followed with extreme caution.

a. Wash hands thoroughly to ensure that excess skin oils are removed, then put on plastic gloves or finger shields.

b. With a dry air or nitrogen source, blow all particulates from the surface to be cleaned.

c. Place a few drops of acetone on a cotton swab until it is saturated. Use the swab to sweep a liquid film of acetone across the optical element from top to bottom. Rotate the swab during the sweep and avoid excessive

contact or pressure on the optical element. Limit the number of sweeps across each element to three over a given area. Use a new swab for each cleaning sweep.

APPENDIX

SYSTEM OPTIMIZATION

Prior to the recommendation and selection of a final laser sensor system design, a number of tradeoff studies were made to establish the most appropriate and cost-effective approach that in our judgment would meet the objectives of the contract. Selection of an air-cooled, sealed laser was made at the onset because of the requirement for an easy to maintain, rugged, fieldable device. Decisions regarding direct versus heterodyne detection, type of laser, and detector required more detailed considerations that are summarized in the following sections.

A.1 LASER TRADEOFF CONSIDERATIONS

The laser system requires that eight wavelengths be obtainable from common and isotopic CO_2 lasers to detect the presence and quantity of chemical agents over the system line of sight. The wavelengths must be individually selectable from the vibration-rotation manifolds of CO_2, and it is desirable that the laser output beam be of the TEM_{oo} mode to insure optimum far-field irradiance.

The laser pulse-width and power are related to the detection technique employed. Heterodyne receivers require highly stable, narrow-bandwidth laser radiation with high spatial mode purity to optimize mixing efficiency at the detectors. Since heterodyne receivers have a diffraction-limited field-of-view, a highly collimated laser is required to concentrate radiation within the receiver's field-of-view. Direct detection systems, on the other hand, require short pulse-widths to optimize signal-to-noise.

Conventional CO_2 lasers (low pressure, electrically excited) are at a highly advanced state of technology and offer many advantages. Their natural line width is reasonably narrow (50 MHz) and suitable for both direct and heterodyne detection. Bandwidths on the order of 10 kHz are achievable and commercially available. However, wavelength selection required for the laser system is not compatible with such narrow-band lasers due to cavity alterations that are inherently less stable than those used in the narrow-bandwidth devices.

The capillary waveguide CO_2 laser has in recent years attracted great attention. Its primary attributes are small size and nearly continuous wavelength tunability due to pressure broadening of the laser line-widths to the point of overlapping. Their main application appears to be in relation to integrated optics and communications. Their mode properties do not appear suitable for long path measurements, and their wide bandwidths place difficult requirements of IF amplifiers used in heterodyne receivers.

Lead salt diode lasers are quite attractive due to their wavelength tunability and extreme spectral purity ($\Delta\nu \sim 10^{-5}$ cm $^{-1}$). However, these lasers are at a relatively early stage of development and require cryogenic cooling (in some cases to 4.2°K) to obtain microwatts of power (mW levels have been achieved at isolated wavelengths). Their output beams are severely divergent (5° x 30° typically) and require anamorphic collimating optics and spectral filtering to obtain single-frequency output.

Spin-flip Raman lasers and optical parametric oscillators (or amplifiers) are suitable laser sources for laboratory studies but are not as yet developed to the stage required for field applications.

A summary of the available laser sources is given in Table A-1.

TABLE A-1. LASER SOURCES AND SUITABILITY TO THE CO_2 LASER SENSOR SYSTEM

Laser	Direct Detection	Heterodyne Detection
Conventional CO_2 (Electronic discharge)	Excellent	Excellent (single λ only)
Capillary Waveguides	Good	Questionable (Linewidth)
Lead Salt Diodes	Poor	Good (limited P_{LO})
Spin-flip Raman	Good (Lab. only)	Poor
Optical Parametric Osc./Amp.	Good (Lab. only)	Poor (Linewidth, Stability)

The final choice for this program was a conventional CO_2 laser.

A.2 RECEIVER TRADEOFF CONSIDERATIONS

The theoretical performance of both direct and heterodyne detectors was studied for the CO_2 laser receiver application. It was recognized that both techniques could be successfully applied to meet the current and future system performance goals based upon sensitivity and signal-to-noise. Therefore, in making a recommendation for a final design, the practical performance limits, cost and technical risk of the alternate methods of detection were evaluated. A discussion of the performance limits of direct and optical heterodyne detection are given in the next two sections, followed by a discussion of the practical tradeoff considerations that led to the recommendation of the final receiver selection.

A.2.1 Direct Detection

The general expression for the conversion of an incident photon stream of average power (P_{opt}) and optical frequency (ν) into a primary photocurrent (I_{ph}) is

$$I_{ph} = \eta q P_{opt}/h\nu$$

with $P_{opt}/h\nu$ = average number of incident photons per unit time, I_{ph}/q = average number per unit time of electron-hole pairs collected across the junction region of a photodiode, or mobile electrons and holes excited within the photoconductor, and η = conversion or quantum efficiency.

The signal-to-noise ratio and the minimum detectable signal are major criteria by which the sensitivity of detection systems to weak optical signals is judged. The S/N at the output of a generalized direct photodetection system that comprises a photodetector with internal current gain (M) and a load circuit as shown in Figure A-1 is given by

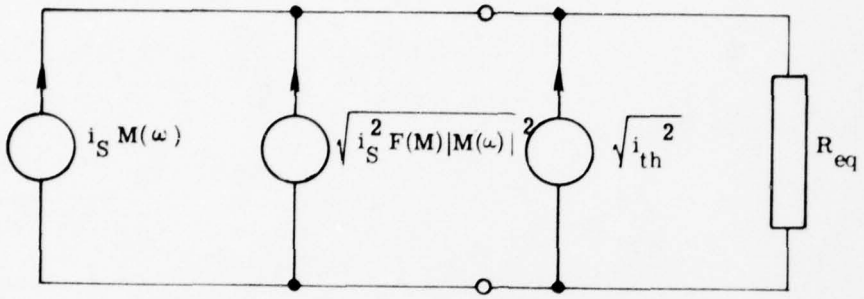

Figure A-1. Equivalent Circuit of Generalized Photodetection System Showing Principal Signal and Noise Sources of Photodetector and Load Circuit

$$\frac{S}{N} = \frac{\frac{1}{2}(mI_{ph})^2 |M(\omega)|^2}{\left[2q(I_{ph} + I_B + I_D)|M(\omega)|^2 F(M) + 4k\frac{T_{eff}}{R_{eq}}\right]B} \qquad (A-1)$$

In this equation, m = modulation index of the light, $M(\omega)$ = current gain or multiplication factor within the photodetector, $2q(I_{ph} + I_B + I_D)B = i_s^2$ = mean-square shot-noise current, I_B = background radiation induced photocurrent, I_D = dark current component that is multiplied within photodetector, B = electrical bandwidth of detection system, and F(M) = factor that accounts for the increase in noise induced by the internal current gain process. The term $4k(T_{eff}/R_{eq})B$ represents the effective mean-square thermal noise current, with R_{eq} being the equivalent resistanceof the photodetector and output circuit, and T_{eff} is an effective noise temperature that takes into account thermal noise due to the detector and noise temperature that takes into account thermal noise due to the detector and load resistor, if any, and the following amplifier. The factor F(M) accounts for the increase in noise that is induced by the current gain process. This noise factor is unity in reverse-biased, solid-state photodiodes. For photoconductors and unbiased photodiodes, F = 2 at low frequencies because the magnitude of the radiation induced generation-recombination noise is twice as large as the shot noise.

From Eq. (A-1) the minimum signal that can be detected for a given bandwidth and signal-to-noise ratio can be determined. With a direct detection system, the highest sensitivity is reached if the minimum detectable signal is limited by fluctuations in the average signal current itself. In this limit, the peak value of the minimum detectable optical power becomes

$$P_{s\ min} = mP_{opt} = 4h\nu \frac{B}{m}\left(\frac{S}{N}\right)\frac{F}{\eta} \qquad (A-2)$$

where Eq. (A-2) is the quantum noise-limited sensitivity of direct detection.

In practical broad-band direct photodetection systems without internal current gain, the minimum detectable signal is usually limited by the thermal noise of the detector and load resistance and by amplifier noise

$$P_{s\ min} = mP_{opt} = \frac{h\nu}{q}\left[B\left(\frac{S}{N}\right)\right]^{1/2}\left(\frac{8kT_{eff}}{\eta^2 R_{eq}}\right)^{1/2} \qquad \text{(A-3)}$$

(thermal or amplifier noise-limited sensitivity).

An appreciable improvement in sensitivity over the thermal or amplifier noise limited case, Eq. (A-3), is possible through the use of photodetectors with internal current gain such as photoconductors. In a practical photodetection system with internal current gain, the highest sensitivity will be reached when the shot noise (which is induced by the average light signal, the background radiation, and the leakage currents) is multiplied to a level comparable to the thermal or amplifier noise. For this optimum current gain (M_{opt}), the minimum detectable signal will be lower by approximately a factor of $2\sqrt{M_{opt}}$ as compared to the thermal noise-limited case without gain, Eq. (A-3).

Sufficient current gain as determined by the previously mentioned noise considerations cannot be reached in all wide bandwidth detection systems because gain-bandwidth limitations ($M \cdot B$) of the current amplification mechanism set an upper limit to the maximum achievable gain M_{max}. In this case, the sensitivity increases only by a factor $\sqrt{M_{max}}$.

In detection systems with moderate bandwidths, both those with and without current gain, the sensitivity is often not limited by thermal or signal induced noise but by noise generated by background radiation (I_B). Noise due to leakage currents are of importance in photodiodes. Noise due to background radiation often sets the sensitivity limit in direct detection systems that operate at infrared wavelengths. However, by limiting the size, spectral acceptance bandwidth, and field of view of the detector and through cooling, these currents can be usually lowered considerably. Temporal discrimination, in conjuction with pulsed laser sources, can greatly reduce background noise contributions whose components are usually of much lower frequency.

4.2.2 Optical Heterodyne Detection

Optical heterodyne receivers have been studied and developed over the last decade, primarily for use in communication systems. They provide excellent sensitivity and signal to noise for such applications. More recently, they have been used for infrared solar radiometry[4] and air pollution detection. The requirements of the laser LOPAIR program can be satisfied by such a system properly designed for the eight specified wavelengths and measurement S/N. The inherent

[4] J.H. McElroy, "Infrared Heterodyne Solar Radiometry," Applied Opt., 11, pp. 1619-1622 (1972).

complexity, both in terms of optical design and signal processing, of such a system and its true performance in the real atmosphere are factors that must be considered.

In optical mixing or heterodyne detection, a coherent optical signal (P_s) is mixed with a laser local oscillator (P_{LO}) at the input of a photodetector as shown schematically in Figure A-2.

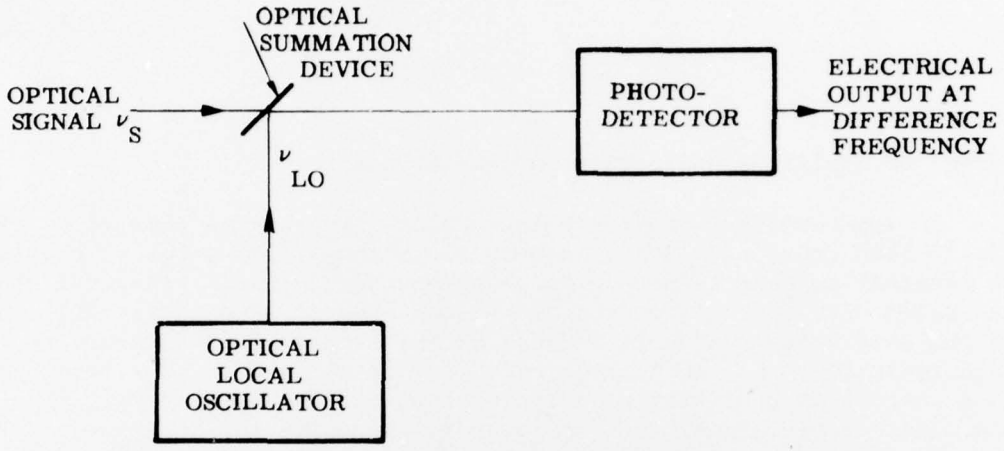

Figure A-2. Optical Heterodyne Detection System

The mean value of the photocurrent generated at the intermidiate or difference frequency for $P_{LO} >> P_s$ is

$$i_{IF} = \frac{\eta q}{h\nu} \sqrt{2P_{LO}P_s} \qquad \text{(A-4)}$$

For the generalized photodetection circuit of Figure A-2, the heterodyne transducer gain (G_T) defined as the ratio of actual IF power delivered to the output amplifier with input resistance (R_A), divided by the available optical signal power (P_s), is

$$G_T = \frac{P_{IF}}{P_s} = 2\left(\frac{\eta q}{h\nu}\right)^2 P_{LO} \frac{(M(\omega)R_{eq})^2}{R_A} \qquad \text{(A-5)}$$

This equation indicates that high conversion gain is possible using sufficient local oscillator power.

For proper mixing action and for best response at the intermidiate frequency, the polarizations of the signal and the local oscillators should be the same. The signal and the local oscillator must both be normally incident and maintain parallel wavefronts over the entire sensitive area of the detector, the dimensions of which should be minimized to ease the alignment requirement. The minimum detectable signal is then as determined from Eq. (A-2) replacing

$mI_{ph}\sqrt{2}$ by i_{iF}, so that $m = 2\,(P_s/P_{LO})^{1/2}$

$$P_{s\ min} = \frac{S}{N} B \left\{ h\nu \frac{F}{\eta} + \left(\frac{h\nu}{q\eta}\right)^2 \frac{1}{P_{LO} M^2} \cdot \left(2k \frac{T_{eff}}{R_{eq}} + qI_B M^2 F\right) \right\} \qquad \text{(A-6)}$$

(sensitivity of heterodyne detection).

For sufficient LO power, the second term representing thermal noise of detector, load, and amplifier, and shot or generation-recombination noise due to background, becomes small. This is the case of a well-designed heterodyne receiver in which noise is dominated by local oscillator-induced shot or generation-recombination noise.

Heterodyne detection thus, in principle, allows realization of optical receivers with wide bandwidths and high sensitivity almost equal to the theoretical quantum noise limit ($h\nu B$). The availability of high conversion gain considerably eases the design requirements for photodetectors. High quantum efficiency and sufficient speed of response of the photodetector and the output circuit are necessary, but the internal current gain is not. Operation at higher temperature than direct detection may also be possible.

Practical application of heterodyne detection is most successful at infrared wavelengths because the alignment requirements are easier to maintain. For 10.6μm, where strong and stable single-line local oscillators exist, heterodyne detection systems with 1-GHz base-bandwidth and with sensitivities that approach the ideal limits have been reported.

The practical performance limits of heterodyne receivers were reviewed. A typical receiver is shown in Figure A-3. If the local oscillator power is selected so that noise terms proportional to P_{LO} dominate all others, the power signal-to-noise ratio at the IF amplifer output is given by:

$$\left(\frac{S}{N}\right)_{IF} = \frac{\left(\frac{\eta P_s}{2h\nu B_{IF}}\right)}{1 + \left(\frac{\eta P_B}{2h\nu B_{IF}}\right)} = \frac{P_s}{P_B + \frac{2h\nu B_{IF}}{\eta}} \qquad \text{(A-7)}$$

Note that for background greater than $2h\nu B_{IF}/\eta$, the background reduces the $(S/N)_{IF}$; that is, we have signal suppression by background.

Davenport and Root[5] show that this (S/N) is not necessarily transferred linearly through the second detector because

$$\left(\frac{S}{N}\right)_{output} = \frac{(S/N)^2_{IF}}{1 + 2(S/N)_{IF}} \qquad \text{(A-8)}$$

Figure A-4 is reproduced from reference 5.

This signal-to-noise degradation at the second detector is sometimes referred to as signal suppression by noise and is due to the nonlinear response of the second detector. For receivers in which $B_{IF} >> B_o$, the output power signal-to-noise ratio then becomes:

$$\left(\frac{S}{N}\right)_{\substack{output \\ power}} = \left(\frac{S}{N}\right)_{\substack{IF \\ power}} \times \frac{B_{IF}}{B_o} \qquad \text{(A-9)}$$

By substitution, the output signal-to-noise ratio then becomes

$$\left(\frac{S}{N}\right)_{\substack{output \\ power}} = \frac{P^2_s(B_{IF}/B_o)}{\left(P_B + \frac{2h\nu B_{IF}}{\eta}\right)^2 + 2P_s\left(P_B + \frac{2h\nu B_{IF}}{\eta}\right)} \qquad \text{(A-10)}$$

For: $P_s \Big/ \left(P_B + \frac{2h\nu B_{IF}}{\eta}\right) >> 1$, $\left(\frac{S}{N}\right)_{out} \longrightarrow \frac{(P_s B_{IF}/B_o)}{2\left(P_B + \frac{2h\nu B_{IF}}{\eta}\right)}$

and $P_s \Big/ \left(P_B + \frac{2h\nu B_{IF}}{\eta}\right) << 1$, $\left(\frac{S}{N}\right)_{out} \longrightarrow \left[P_s \Big/ P_B + \frac{2h\nu B_{IF}}{\eta}\right]^2 (B_{IF}/B_o)$

In addition to the sensitivity limit for heterodyne detection, there is a field-of-view limit spelled out by Siegman[6]:

$$A_R \, \Omega_r = \lambda^2 \qquad \text{(A-11)}$$

where:

A_r = receiver input aperture area

Ω_r = receiver field of view solid angle

λ = wavelength

[5] Davenport and Root, Random Signals and Noise, Chapter 12, McGraw-Hill (1958).

[6] A. Siegman, The Antenna Properties of Optical Heterodyne Receivers, Proc IEEE, Oct. 1066.

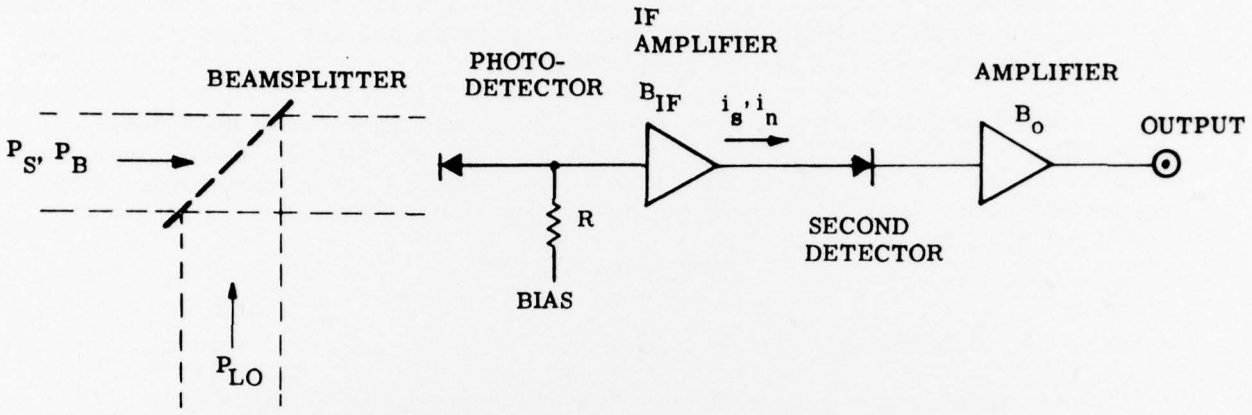

Figure A-3. Heterodyne Receiver Functional Diagram

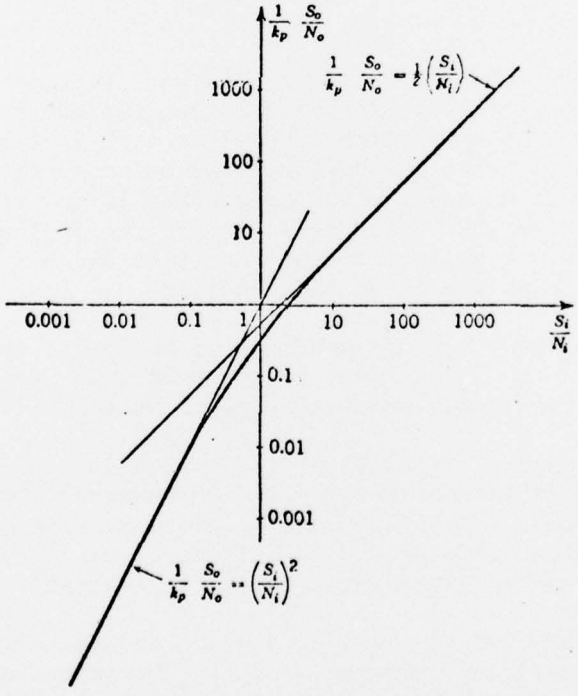

Figure A-4. Output Signal-to-Noise Power Ratio versus Input Signal-to-Noise Power Ratio for a Full-Wave Square-Law Detector

This is caused by the coherence requirement at the optical detector and, in effect, says that the field of view of a heterodyne receiver is limited to the diffraction-limited field of the antenna. This limit can only be overcome by parallel detector-amplifier-channels or by image plane mixing with a large detector and with a significant loss in S/N.

There are many practical pitfalls in the use of optical heterodyne detection. One severe limitation is indicated by Eq. (A-10), which shows that because the IF SNR is almost always very small due to large bandwidths, overall equivalent noise bandwidth for the zero background case is

$$(B_{IF} \times B_o)^{1/2}$$

A very wide IF bandwidth will be required if:

a. the transmitter or LO is slightly unstable or noisy

b. the backscattering medium is moving so as to generate Doppler modulation

In principle this limitation may be overcome by the use of a heterodyne second detector with a phase-lock loop controlling the second local oscillator. However, this can only be done under very stable conditions.

The transmitter and receiver optics must be very stable because there are many places where slight microphonics can introduce spurious noise. Figure A-5 shows a few of these in which a very small reflection will cause local oscillator energy to reach the detector via an unwanted path. Phase modulation of this path then causes phase modulation of the reflected energy. If the frequency spectrum of this noise falls within the IF bandwidth, it will appear in the receiver output as spurious noise. Also shown in Figure A-5 are places where electronic noise can enter the receiver.

Figure A-6 shows a crude estimate of the power spectra for various known spuroius noise sources. This must be measured under actual conditions before numerical values can be placed on the coordinates of Figure A-6.

Another category of practical limitation in an optical heterodyne receiver is caused by the requirement for coherent wavefronts (LO ref. signal) at the detector. This means that high quality optics must be used; but more significantly, it means that atmospheric turbulence can cause severe degradation of S/N. This has been discussed extensively in the literature[7].

If the transceiver is moving relative to the target scatterer, there will be a Doppler shift of the detected energy. The impact of this effect is discussed in reference [8]. Doppler effects will only be encountered if high-speed spatial scanning or measurements from a moving platform are attempted.

---

[7] D. Fried, "Optical Heterodyne Detection of an Atmospherically Distorted Signal Wavefront", Proc. IEEE (Jan. 1967).

[8] R. Crane, "Heterodyne Detection for Laser Camera", Perkin-Elmer Report No. 9848 (Jan. 1970).

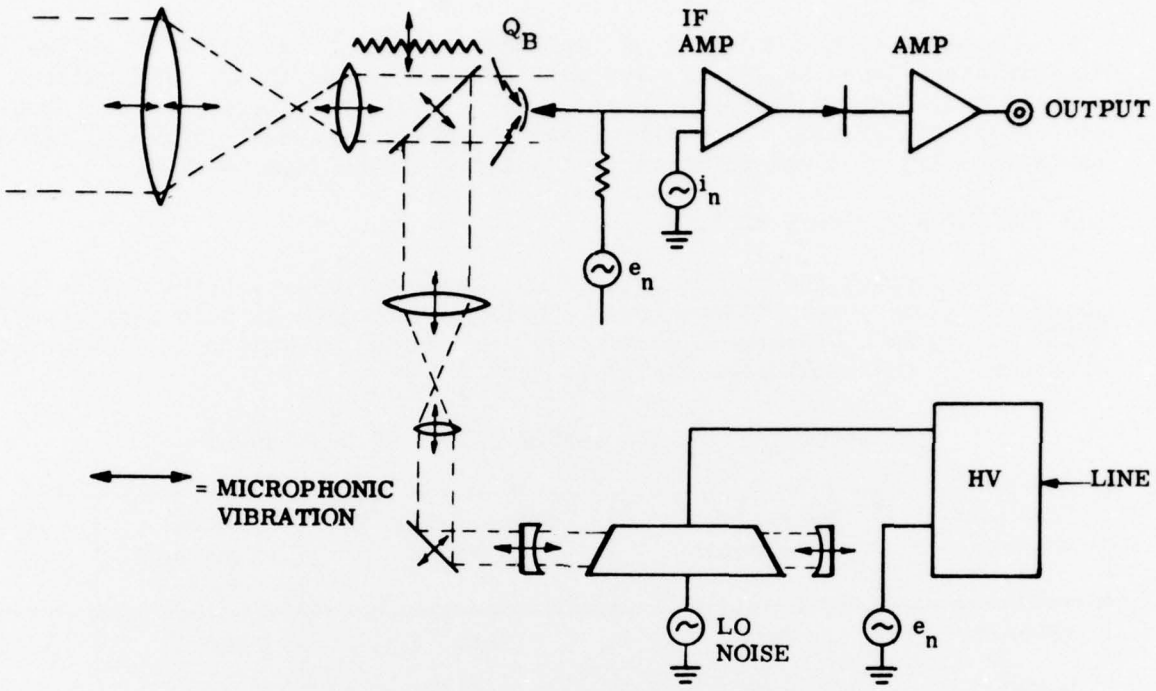

Figure A-5. Sources of Spurious Noise in a Heterodyne Receiver

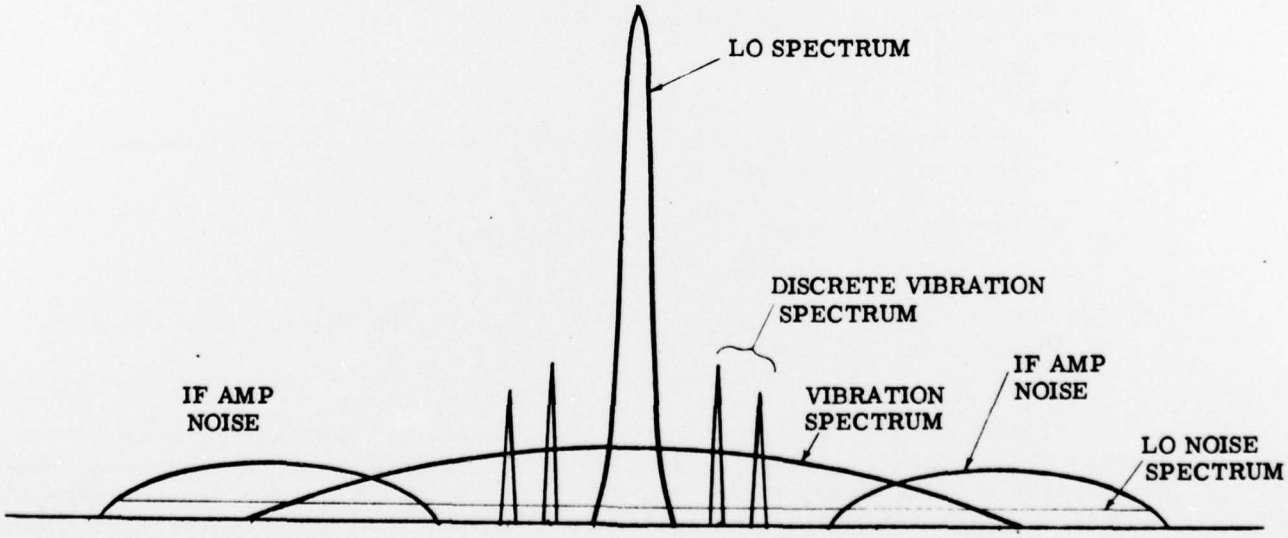

Figure A-6. Crude Representation of Spurious Noise Spectra in a Heterodyne Receiver

Finally, the complexity of implementing such a detection technique for six different local oscillator frequencies must be mentioned. This places rather difficult requirements on the laser (local oscillator) and the stability of the optical system. These requirements were considered a serious disadvantage in light of the required fieldability of the laser system.

A.3 DETECTOR TRADEOFF RESULTS

The wavelengths of interest in CO_2 laser energy detection lie in the range of 9-11μm. The IR detectors capable of detection in this region under 300°K photon flux background conditions are listed in Table A-2. The detector size for all the candidates listed is 1 mm x 1 mm.

TABLE A-2. LASER SENSOR DETECTION CANDIDATES

Detector Material	Operating Temperature	Detectivity, D* cm $Hz^{\frac{1}{2}}/w$	Time Constant sec	Cost in $
(PbSn)Te	77°K	2.5×10^{10} (Pv)	3×10^{-7}	~ 3.5K
HgCdTe	77°K	2.5×10^{10} (Pc)	5×10^{-7}	~ 4K
		1×10^{10} (Pv)	10^{-7}	
Ge:Hg	< 30°K	1×10^{10} (Pc)	~ 10^{-8}	≥ 5K
Pyroelectric Detectors (TGS, PVF_2 Niobated)	300°K	3×10^{8}	- 10^{-3}*	≤ 1K

P_c = Photoconductive mode

P_v = Photovoltaic mode

*The time constant is essentially determined by the thermal time constant of the detector material.

From Table A-2, we can conclude the following. Although pyroelectric detectors are relatively inexpensive and offer room-temperature operation, they do not have a large enough bandwidth required for the CO_2 laser sensing system (except as laser reference detectors). The bandwidth of pyroelectric detectors can be increased at the price of drastic decreases in sensitivity. Mercury-doped germanium mertis the bandwidth and the detectivity requirements but must be operated below 30°K temperature. This temperature requirement makes it unsuitable. The choice of detector material is limited to (HgCd)Te or (PbSn)Te.

The photoconductive (HgCd)Te has the required D* and the bandwidth. However, the photoconductive (HgCd)Te detector must be brazed to obtain a high D*. It also has a substantial 1/f noise up to 1 KHz, which is bias dependent and will contribute significantly to the signal-to-noise ratio measured under large bandwidth conditions. The photoconductive (HgCd)Te detector does not require bias and has considerably less 1/f noise. However, it has a lower D* value than the photoconductive detectors. The higher D* photoconductive (HgCd)Te detectors can be obtained through a selection process that can increase its cost considerably.

The lead-tin-telluride detectors appeared to meet all the system requirements. They are photovoltaic; hence, no bias is required. They have the appropriate D* and bandwidth and are moderately priced. For these reasons a (PbSn)Te photovoltaic detector was used in the final system.

A.4 ATMOSPHERIC TURBULANCE AND SPECKLE EFFECTS

During the study, an evaluation was made of the effects of scintillation and laser speckle on system performance. The laser beam divergence and receiver field-of-view were then selected to minimize these sources of error.

When a diffusely scattered laser spot is observed, it has a speckle appearance which usually changes quite rapidly with time. The speckled appearance of the laser light is caused by the constructive or destructive interference of light scattered along paths of varying length. Because laser light is so coherent, light from spatially separated scattering elements can interfere with each other. Very small changes in the geometry (on the order of a wavelength) will cause the speckle pattern to change. Thus, Brownian motion of aerosol scatterers or small vibrations of solid diffuse scatterers will cause the speckle pattern to change in time. Even though the displacement of the scatterers may be slow, the time required to traverse one wavelength is usually quite short typically less than 100 μsec. Thus, one can anticipate that the speckle pattern will be completely changed from pulse to pulse.

The size of a single speckle spot at the receiver from a source subtending an angle α is

$$\frac{1.22\lambda}{\alpha} \qquad \text{(A-12)}$$

The intensity of this spot size will be 100% modulated according to an exponential probability distribution. Since a receiver of aperture D subtends

$$\frac{\frac{\pi}{4} D^2}{(1.22\lambda/\alpha)^2} \qquad \text{(A-13)}$$

speckle spots, the total intensity received will exhibit rms fluctuations of

$$\frac{\text{rms speckel fluctuations in intensity}}{\text{average intensity}} = \frac{1.38\lambda}{D\alpha} \qquad \text{(A-14)}$$

and these fluctuations will obey a Poisson probability distribution. Using $\lambda = 10\mu$, D = 30 cm and α = 1 mrad gives rms fluctuations of 4.6%. The rms fluctuations are plotted versus α and D in Figure A-7. The laser speckle can be reduced by increasing D and/or α.

In addition to laser speckle, the received intensity will scintillate due to atmospheric turbulence along the path. The turbulence causes varying optical path lengths, which result in interference between rays traversing different paths. Intensity fluctuations caused by this interference are called scintillation.

For a point source and a point receiver, the rms fluctuations in the logarithm of the received intensity, σ, (i.e., $I \sim e^{\sigma}$) are found from the equation

$$\sigma^2 = 4 \cdot (2\pi k)^2 \int_{\sim}^{\infty} KdK\, F_A(K) \qquad \text{(A-15)}$$

where $k = 2\pi/\lambda$, K = spatial frequency (radians/meter), and $F_A(K)$ is the spatial Weiner spectrum of the scintillation, $F_A(K)$ is given by (9)

$$F_A(K) = \int_o^R dZ\, \phi(K,Z)\, \sin^2\left[\frac{K^2 Z(R-Z)}{2kR}\right] \frac{R^2}{(R-Z)^2} \qquad \text{(A-16)}$$

where $\phi(K,Z)$ is the index 3 dimensional Weiner spectrum at a distance Z from the receiver, and R is the total range. These equations are valid for $\sigma<2$, at about which point saturation effects set in. For Kolmogorov turbulence, ϕ has the form

$$\begin{aligned} \phi(K,Z) &= 0.033\, C_n^2(Z)\, K^{-11/3} && K < Km \\ &= 0 && K > Km \end{aligned}$$

where Km corresponds to the inner scale turbulence (about 10^3 cycles/m), and $C_n(Z)$ is the index structure function ($\tilde{}10^{-7}$ cm $^{-1/3}$ at 2 meter heights).[10] Integration of the above equations show that saturation effects will start to appear in the 0.5 km to 1 km range. At longer ranges, the shape of F_A will change and the statistics will gradually change from a log normal distribution to an exponential distribution. Actually, one cannot ever have a path long enough on earth to ever fully reach the exponential distribution. Rather the fluctuations will follow a modified log-normal distribution.

In practice, one does not have point sources and point receivers, but rather sources of finite extent and receivers of finite extent. This modifies F_A as follows:

---

[9] From equation 9.27 in Tatarski. (Wave Propagation in a Turbulent Media McGraw-Hill 1961) with $\frac{KL}{\eta} = K'$; $\eta = L-Z$; L=R.

[10] Tatarski - Ibid, p. 215.

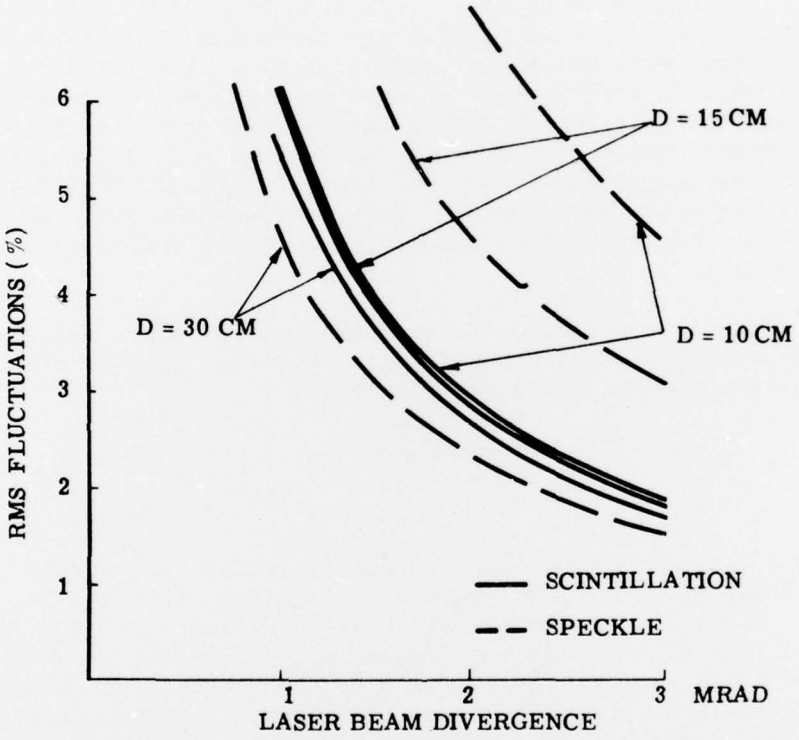

Figure A-7. RMS Atmospheric Scintillation and Laser Speckle Fluctuations as a Function of the Laser Beam Divergence, α, for Various Receiver Diameters, D.

$$F_A(K) = \int_o^R dZ\ \phi(K,Z)\ \sin^2\left[\frac{K^2Z(R-Z)}{2kR}\right] H_1\left(\frac{\alpha KZ}{2}\right) H_2\left[\frac{KD}{2}\left(\frac{R-Z}{R}\right)\right] \frac{R^2}{(R-Z)^2}$$

(A-17)

Here H_1 is the spatial filter function due to the source subtending an angle α, while H_2 is the spatial filter function due to the receiver having an aperture D. We take H_1 to be the filter function for a uniform beam of circular cross section (i.e., we neglect the intensity variations in the laser spot due to atmospheric turbulence along the path from the laser to the target under the assumption that such turbulence is small and will average out since all the light on the target is within the receiver field of view). We also assume a circular receiver aperture. Under these assumptions, the above equations can be integrated (with some approximations) to give a value of $\sigma = 5.5\%$ for the above parameters. The variation of σ and α and D is given in Figure A-7. In general, the atmospheric scintillation can be decreased by increasing D or α.

The temporal correlation between successive pulses will be determined by the wind velocity. The characteristic frequency (f_c) of atmospheric turbulence is given theoretically-empirically by

$$f_c = \frac{0.32\ \bar{\nu}_n}{(\lambda R)^{\frac{1}{2}}} \qquad \text{(A-18)}$$

where $\bar{\nu}_n$ is the average wind velocity normal to the light path. Experimental results indicate that the dependence on R is slower than this equation would indicate.[11] The value of f_c will be about 16 Hz for a 7.6 mph normal wind velocity. A plot of the expected frequency distribution is shown in Figure A-8. We note that even though the peak of the curve is at 16 Hz, the spectrum contains considerable power at higher frequencies. While the exact temporal correlation between successive pulses can be obtained from Figure A-8 by transferring the frequency spectrum on a computer, we can roughly estimate the correlation time from

$$\tau_c \simeq 1/2\pi f_c$$

to be 0.01 sec. This is also the time between successive pulses at the same wavelength. Thus we expect some correlation (about 37%) between successive pulses for normal wind velocities less than 7.6 mph. This correlation between successive pulses indicates that more pulses will be required to achieve a statistical average than might be anticipated. An estimate of the reduction of the rms scintillation versus the number of pulses and wind speed is shown in Figure A-9.

---

[11] D.H. Hohn, Applied Optics, 5, 1966, pp. 1433-1436. He finds $f_c \nu_n = 0.131$ cm in the visible, which is equivalent to Tatarski's formula for L = 1000 m.

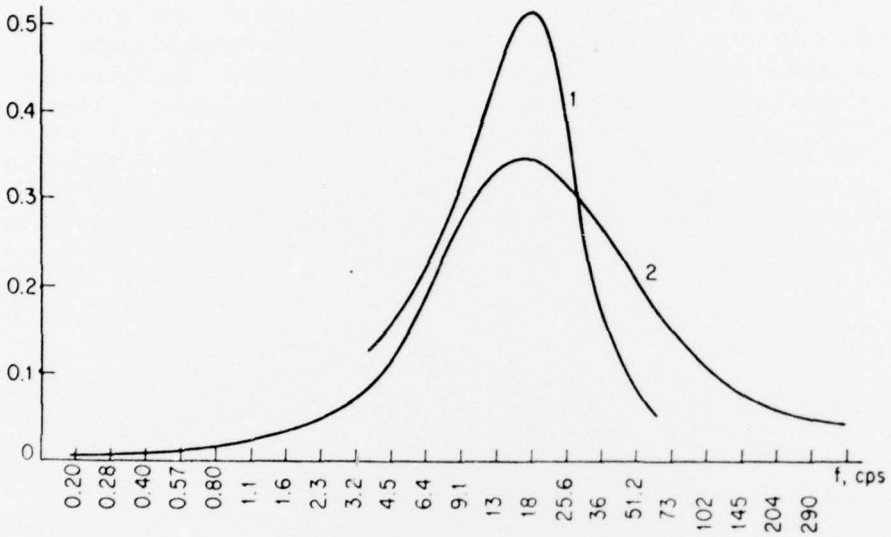

Figure A-8. The Atmospheric Scintillation Frequency Spectra for 7.6 mph Nominal Wind Velocity

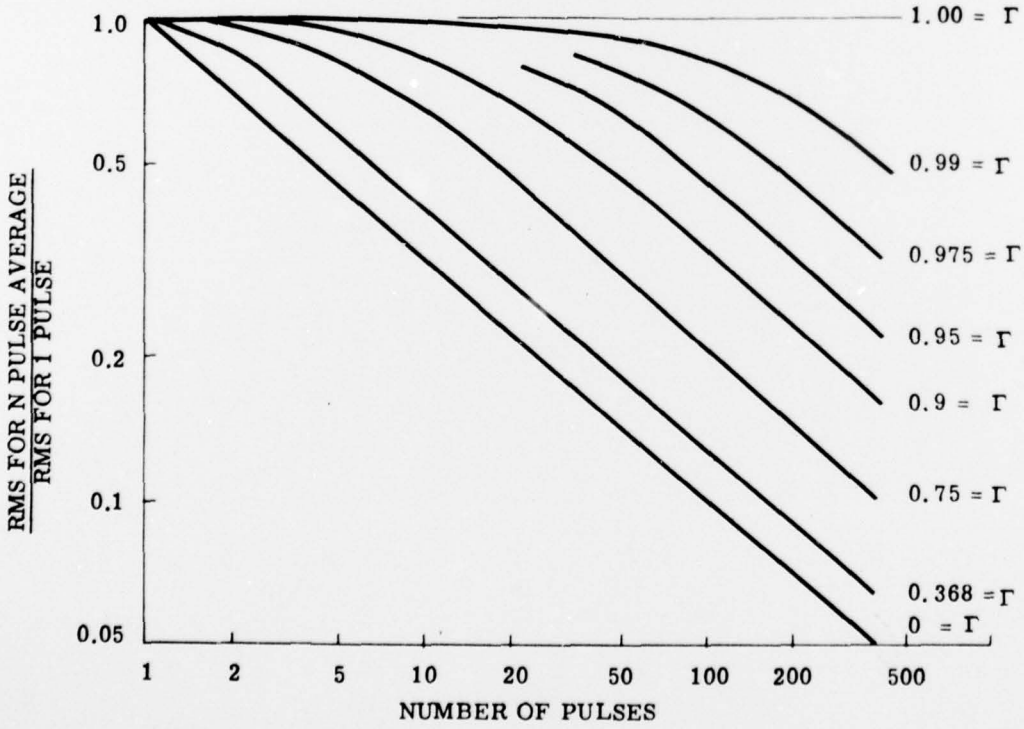

Figure A-9. Effects of the Correlation Coefficient $\Gamma = \exp[-2\pi f_c \tau]$ on N Pulse Averaging to Reduce the rms Scintillation Fluctuations for the System Discussed in the Text $\tau = 0.01$ sec and $f_c \approx 2.08\ \bar{\nu}$/mph.

The speckle fluctuations and the atmospheric scintillation fluctuations obey different statistics (Poisson and modified log normal) so that the total fluctuations is not, strictly speaking, the rms of the speckle and scintillation fluctuations. However, as the speckle and scintillation fluctuations are small, they must be very nearly normal (i.e., these distributions approach the normal distribution in the limit of small fluctuations or large numbers). For a 10 mph wind, 30-cm receiver, and 2.5-mradian beam, fc $\approx$ 2.1 Hz and the correlation coefficient $\approx$ 2.8. From Figure A-9 an average of 10 pulses will reduce the 2% fluctuation of a single pulse to a value less than 1%. For the 1.67 time constant of the signal processing integrating filter, the effects of scintillation will become insignificant.

DISTRIBUTION LIST

Recipient	Number of copies
Defense Documentation Center ATTN: DDC-IRS Cameron Station Alexandria, Virginia	12
Commander Edgewood Arsenal Attn: SAREA-DE-DDR (V. James Cannaliato) Aberdeen Proving Ground, Maryland 21010	30

Copies	Addressee
1	Technical Director, Attn: SAREA-TD
1	Director of Dev & Engr, Attn: SAREA-DE
1	Director of Dev & Engr, Attn: SAREA-DE-DD
1	Director of Dev & Engr, Attn: SAREA-DE-DDR
1	Director of Dev & Engr, Attn: SAREA-DE-DB
13	Contract Project Officer
1	Alternate Contract Project Officer
3	Director of Tech Spt, Attn: SAREA-TS-L (Bldg E3330)
1	Director of Tech Spt, Attn: SAREA-TS-E
1	Director of Tech Spt, Attn: SAREA-TS-R
1	Director of Cml Lab, Attn: SAREA-CL-PD (Dr. Epstein)
1	Director of Cml Lab, Attn: SAREA-CL-CA (Mr. Sass)
1	CG, USA Material Development & Readiness Command, Attn: DRCDE, Washington, DC 20315
1	Commander, US Army Armament Command, Attn: DRSAR-RDM, Rock Island, Illinois 61201
1	Commander, US Army Armament Command, Attn: DRSAR-RDT, Rock Island, Illinois 61201
1	Commander, Naval Weapons Laboratory Attn: Code FC, Dahlgren, Virginia 22448